

Dalton Transactions

Accepted Manuscript



This article can be cited before page numbers have been issued, to do this please use: S. S. Massoud, C. C. Ledet, T. Junk, S. Bosch, P. Comba, R. Herchel, J. Hošek, Z. Travnicek, R. Fischer and F. A. Mautner, *Dalton Trans.*, 2016, DOI: 10.1039/C6DT02596J.



This is an *Accepted Manuscript*, which has been through the Royal Society of Chemistry peer review process and has been accepted for publication.

Accepted Manuscripts are published online shortly after acceptance, before technical editing, formatting and proof reading. Using this free service, authors can make their results available to the community, in citable form, before we publish the edited article. We will replace this *Accepted Manuscript* with the edited and formatted *Advance Article* as soon as it is available.

You can find more information about *Accepted Manuscripts* in the [Information for Authors](#).

Please note that technical editing may introduce minor changes to the text and/or graphics, which may alter content. The journal's standard [Terms & Conditions](#) and the [Ethical guidelines](#) still apply. In no event shall the Royal Society of Chemistry be held responsible for any errors or omissions in this *Accepted Manuscript* or any consequences arising from the use of any information it contains.

Dinuclear metal(II)-acetato complexes based on bicompartamental 4-chlorophenolate: syntheses, structures, magnetic properties, DNA interactions and phosphodiester hydrolysis[†]

Salah S. Massoud,^{*a} Catherine C. Ledet,^a Thomas Junk,^a Simone Bosch,^b Peter Comba,^{*b} Radovan Herchel,^c Jan Hošek,^c Zdeněk Trávníček,^{*c} Roland C. Fischer,^d Franz A. Mautner,^{*e}

^a*Department of Chemistry, University of Louisiana at Lafayette, Lafayette, LA 70504, U. S. A.*

^b*Anorganisch-Chemisches Institut and Interdisziplinäres Zentrum für Wissenschaftliches Rechnen (IWR), Universität Heidelberg, Im Neuenheimer Feld 270, 69120 Heidelberg, Germany*

^c*Department of Inorganic Chemistry & Regional Centre of Advanced Technologies and Materials, Faculty of Science, Palacký University, 17. listopadu 12, CZ-77146 Olomouc, Czech Republic*

^d*Institut für Anorganische Chemie, Technische Universität Graz, Stremayrgasse 9/V, A-8010 Graz, Austria*

^e*Institut für Physikalische and Theoretische Chemie, Technische Universität Graz, Stremayrgasse 9/II, A-8010, Graz, Austria*

Received:

Accepted:

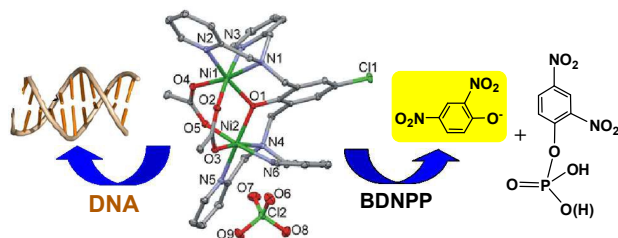
Keywords: Dinuclear complexes / Bridged phenolate / Crystal structures / Magnetic properties / Phosphodiester hydrolysis / DNA interactions

[†] CCDC 1444958-1444963 contain the supplementary crystallographic data for complexes **1** - **6**, respectively. These data can be obtained free of charge from via the Internet at <http://pubs.acs.org>. Crystallographic data and processing parameters, and selected bond parameters for compounds **1** – **6** are summarized in Tables S1 and S2-S7, respectively. Possible hydrogen bonds for compounds **1** and **4** are given in S8, respectively. The ¹H and ¹³C NMR spectra for complex **5** are illustrated in Figures S1 and S2, respectively and atom numbering scheme is shown in Chart S1. The magnetic data of complex **2**, and the incubation data time for complex **3** with DNA, are shown in Figures S3 and S4, respectively.

* To whom correspondence should be addressed. E-mail: ssmassoud@louisiana.edu, Tel. +01 337-482-5672, Fax: +01 337-482-5676 (S. S. Massoud); E-mail: peter.comba@aci.uniheidelberg.de, Tel. +49-6221-548453, Fax: +49-6221-546617 (P. Comba); E-mail: zdenek.travnicek@upol.cz, Tel. +420 585-634-352, Fax: +420 585-634-954 (Z. Trávníček); mautner@tugraz.at, Tel: ++43-316-873-32270, Fax: ++43-316-873-8225 (F. A. Mautner)

ABSTRACT

A series of dinuclear metal(II)-acetato complexes: $[\text{Ni}_2(\mu\text{-L}^{\text{ClO}})(\mu_2\text{-OAc})_2](\text{PF}_6) \cdot 3\text{H}_2\text{O}$ (**1**), $[\text{Ni}_2(\mu\text{-L}^{\text{ClO}})(\mu_2\text{-OAc})_2](\text{ClO}_4) \cdot \text{CH}_3\text{COCH}_3$ (**2**), $[\text{Cu}_2(\mu\text{-L}^{\text{ClO}})(\mu_2\text{-OAc})(\text{ClO}_4)](\text{ClO}_4)$ (**3**), $[\text{Cu}_2(\mu\text{-L}^{\text{ClO}})(\text{OAc})_2](\text{PF}_6) \cdot \text{H}_2\text{O}$ (**4**), $[\text{Zn}_2(\mu\text{-L}^{\text{ClO}})(\mu_2\text{-OAc})_2](\text{PF}_6)$ (**5**) and $[\text{Mn}_2(\text{L}^{\text{ClO}}\text{-O})(\mu_2\text{-OAc})_2](\text{ClO}_4) \cdot \text{H}_2\text{O}$ (**6**), where $\text{L}^{\text{ClO}}\text{-O}^- = 2,6\text{-bis}[\text{bis}(2\text{-pyridylmethyl})\text{aminomethyl}]\text{-4-chlorophenolate}$, were synthesized. The complexes were structurally characterized by spectroscopic techniques and single crystal X-ray crystallography. Six-coordinate geometries with doubly bridged acetato ligands were found in Ni(II), Zn(II) and Mn(II) complexes **1**, **2**, **5** and **6**, whereas with Cu(II) complexes a five-coordinate species was obtained with **4**, and mixed five-, and six-coordinate geometries with a doubly bridged dimetal core was observed in **3**. The magnetic properties of the complexes **1-4** and **6** were studied at variable temperature and revealed weak to very weak antiferromagnetic interactions in **1**, **2**, **4** and **6** ($J = -0.55$ to -9.4 cm^{-1}) and ferromagnetic coupling in **3** ($J = 15.4 \text{ cm}^{-1}$). These results are consistent with DFT calculations performed at the B3LYP/def2-TZVP(-f) level of theory. Under physiological conditions, the interaction of the dinuclear complexes **1-5** with supercoiled plasmid ds-DNA did not show any pronounced nuclease activity, but Ni(II) complexes **1** and **2** revealed a strong ability to unwind the supercoiled conformation of ds-DNA. The mechanistic studies performed on the interaction of the Ni(II) complexes with DNA demonstrated the important impact of the nickel(II) ion in the unwinding process. In combination with the DNA study, the phosphatase activity of complexes **1**, **3**, and **5** was examined by the phosphodiester hydrolysis of bis(2,4-dinitrophenol)phosphate (BDNPP) in the pH range of 5.5-10.5 at 25° C. The Michaelis-Menten kinetics performed at pH 7 and 10.7 showed that catalytic efficiencies $k_{\text{cat}}/K_{\text{M}}$ (k_{cat} = catalytic rate constant, K_{M} = substrate binding constant) decrease in the order: Ni(II), **1** > Zn(II), **5** > Cu(II), **3**. Similar trend was also observed with the turnover numbers at pH = 7. The results are discussed in relation to coordination geometry and nature of the metal center as well as the steric environment imposed by the compartmental phenoxido ligand.



Introduction

In the last decade, a large number of bi-compartmental phenolate ligands with symmetrical and asymmetrical pendant chelating arms, including pyridyl and substituted pyridyl groups, attached to the 2- and 6-positions of the phenol ring were synthesized and structurally characterized. These ligands due to their ability to bind two identical or different $3d$ metal ions which are simultaneously bridged through the deprotonated phenolic group resulted in the formation of homo- and hetero-dinuclear metal complexes.¹⁻⁶ In some cases, the presence of hydroxido and acetate ions may lead to further bridge and hence to doubly or triply bridged dinuclear metal complexes where the two metal centers are in close proximity in the range of 2.9-4.0 Å.⁷⁻²¹ Such coordination environments around the central metal ions together with the possible existence of “*coordinatively unsaturated*” metal ion(s) and center with a “*weakly bound*” ligand(s) made these complexes attractive targets to mimic the active sites in the biological systems in order to elucidate the mechanism and the structural parameters of metalloproteins e.g. hemocyanin,¹² metallo- β -lactamases (M β L),¹³ catecholase oxidases,^{8,14,15} Mn catalases,^{16,17} and the phosphodiester hydrolysis of biomolecules such as purple acid phosphatases, (PAPs), phosphoesterases and DNA nucleases.^{10,15,18-25} In addition to the possible use of these compounds in modeling the biological systems, they provide a wide range of ferro-/antiferro-magnetic coupling between the two paramagnetic metallic centers ($3d^{5-9}$), bridged *via* the phenoxido group and through other ligands, which allows to probe the electronic structure of these compounds and compare them with the natural systems.^{1,9,11,23}

Recently, dinuclear Zn(II), Cu(II), Co(II) and Fe(II) based phenolate systems have been extensively used as “*artificial nucleases*” to study the catalytic hydrolysis of phosphodiester compounds where the close proximity and the geometrical nature around the two metal ions as well possible “*cooperativity*” may enhance the P-O bond rupture.^{15,18-24} The P-O bonds in the phosphodiester linkages of DNA and RNA strands exhibit remarkable stability towards hydrolysis which is one of the most essential requirements for the survival and maintenance of life.²⁶ Under physiological conditions, the half-life $t_{1/2}$ for the hydrolysis of DNA was estimated to be $\sim 130,000$ years.²⁵ This unusual stability of the P-O bonds towards hydrolysis in DNA was overcome in nature by the development of a number of hydrolytic metalloenzymes that efficiently catalyze the hydrolysis of P-O bonds of the DNA phosphate backbone.²⁶ These metalloenzymes contain metal

ions in their active sites. Therefore, modeling of these hydrolytic enzymes is a fundamental step in designing “*artificial nucleases*” capable of competing with natural ones.²⁷⁻³¹

Two mechanistic pathways have been found in the DNA cleavage by small metal complexes. The first mechanism involves oxidative cleavage that occurs via reactive oxygen species (ROS: reactive singlet oxygen, $^1\text{O}_2$; superoxide, O_2^- ; hydroxyl radical, OH^\bullet) and this requires the addition of external agents such as light, oxidative, and/or reductive species to initiate the cleavage.³¹⁻³⁶ Also, this mechanism generates fragments that damage the ribose sugar and/or nucleic bases of the DNA and hence hamper their use *in vivo*.³⁷ The second mechanism is the hydrolytic cleavage that requires the activation of a nucleophile (OH^-) in proximity to the phosphoester moiety,^{30,32,38,39} and this mechanism does not suffer from the drawbacks of the oxidative cleavage mechanism because the generated DNA products can be enzymatically relegated.⁴⁰⁻⁴⁶ However, this raises a question concerning the validity of the substrate compounds generally used to promote the hydrolysis of simple phosphodiester “*model systems*” since the operating mechanism is not necessarily the same and the reactivity might therefore differs significantly.

In addition to the cleavage of the supercoiled circular dsDNA (SC-form or form **I**) to the relaxed open circular form of DNA (OC-form or form **II**) and/or the linear DNA (L-form or form **III**) by small metal(II) complexes,³³⁻³⁹ it is possible that some of these molecules, especially those derived from Ni(II), Cu(II) and Zn(II) can bind DNA in a similar fashion to intercalators and induce single- or double-strand breaks leading to “unwinding” (i.e. relaxing) of SC-DNA to create OC- or L-form of DNA.⁴⁷⁻⁵¹ This binding alters the DNA winding lengthens and stiffens. These structural changes may cause interference in the recognition and function of DNA-binding proteins.⁵¹⁻⁵³

Therefore, we believe that the bicompartamental ligands 2,6-bis[bis(2-pyridylmethyl)aminomethyl]-4-substituted-phenol ($\text{L}^{\text{R}}\text{-OH}$) are suitable candidates to synthesize relevant dinuclear metal(II) complexes. The close proximity of the bridged metal ions may allow their cooperativity and hence enhances the capability of the complexes in promoting the cleavage of P-O bonds in phosphodiester compounds and DNA. Therefore, herein, we report the synthesis and structural characterization of six new dinuclear compounds with additional acetate bridges, $[\text{Ni}_2(\mu\text{-L}^{\text{Cl}}\text{O})(\mu_2\text{-OAc})_2](\text{PF}_6)\cdot 3\text{H}_2\text{O}$ (**1**), $[\text{Ni}_2(\mu\text{-L}^{\text{Cl}}\text{O})(\mu_2\text{-OAc})_2](\text{ClO}_4)\cdot \text{CH}_3\text{COCH}_3$ (**2**), $[\text{Cu}_2(\mu\text{-L}^{\text{Cl}}\text{O})(\mu_2\text{-OAc})(\text{ClO}_4)](\text{ClO}_4)$ (**3**), $[\text{Cu}_2(\mu\text{-L}^{\text{Cl}}\text{O})(\text{OAc})_2](\text{PF}_6)\cdot \text{H}_2\text{O}$ (**4**), $[\text{Zn}_2(\mu\text{-L}^{\text{Cl}}\text{O})(\mu_2\text{-OAc})_2](\text{PF}_6)\cdot \text{H}_2\text{O}$ (**5**), and $[\text{Zn}_2(\mu\text{-L}^{\text{Cl}}\text{O})(\mu_2\text{-OAc})_2](\text{PF}_6)\cdot \text{H}_2\text{O}$ (**6**).

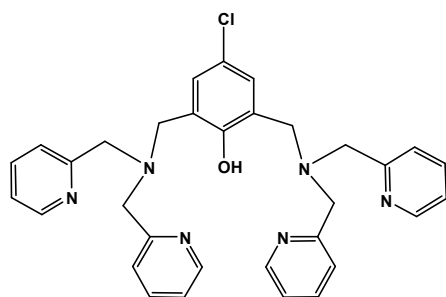
OAc)₂](PF₆) (**5**) and [Mn₂(L^{Cl}-O)(μ₂-OAc)₂](ClO₄)·H₂O (**6**) together with their magnetic properties (**1-5**). The bridged μ-acetato compounds **1**, **3** and **5** were also selected to study the hydrolysis of bis(2,4-dinitrophenyl)phosphate (BDNPP) and the DNA cleavage/unwinding. The reactivity and the mechanistic pathways of these complexes are evaluated and compared to other related systems.

Results and discussion

Synthesis of the complexes

The reaction of a methanolic solution containing 2,6-bis[bis(2-pyridylmethyl)aminomethyl]-4-chlorophenol (L^{Cl}-OH)^{1(a,b)} (Chart 1) and two equivalents of M(OAc)₂·nH₂O (M = Ni, n = 4; M = Cu, n = 1; M = Zn, n = 2) in the presence of NaClO₄ or NH₄PF₆ afforded the dinuclear complexes [Ni₂(μ-L^{Cl}O)(μ₂-OAc)₂](PF₆)·3H₂O (**1**), [Ni₂(μ-L^{Cl}O)(μ₂-OAc)₂](ClO₄)·CH₃COCH₃ (**2**), [Cu₂(μ-L^{Cl}O)(μ₂-OAc)(ClO₄)](ClO₄) (**3**), [Cu₂(μ-L^{Cl}O)(OAc)₂](PF₆)·H₂O (**4**) and [Zn₂(μ-L^{Cl}O)(μ₂-OAc)₂](PF₆) (**5**) in moderate yields (~ 60%) for complexes **1-4** and high yield (90%) for the Zn(II) complex, **5**. [Mn₂(L^{Cl}-O)(μ₂-OAc)₂](ClO₄)·H₂O (**6**) was obtained in 40% yield by the reaction of Mn(ClO₄)₂·6H₂O and L^{Cl}OH in MeOH, followed by the addition of sodium acetate. The complexes are soluble in MeOH, CH₃CN and acetone. However, upon dissolution of the blue complexes **1**, **2** and **4** in CH₃CN there is a color change to green. Single crystals suitable for X-ray structure determination were obtained either directly from the methanolic solutions (**3-5**) or by further recrystallization of the complexes from MeOH (**1**, **6**), whereas X-ray quality single crystals for complex **2** were obtained from recrystallization of the complex from acetone. The isolated complexes were characterized by elemental microanalyses, molar conductivity, IR and UV-VIS spectroscopy and by single crystal X-ray crystallography.

Chart 1. Structural formula of 2,6-bis[bis(2-pyridylmethyl)aminomethyl]-4-chlorophenol



The molar conductivities of the synthesized complexes, Λ_M were measured in CH_3CN and the values are summarized in Table 1. The values ($\Lambda_M = 131\text{-}167 \text{ } \Omega^{-1}\text{cm}^2\text{mol}^{-1}$) reveal the 1:1 electrolytic behavior for complexes **1**, **2**, **4**, **5** and **6**. The color change associated with the dissolution of complexes **1** and **2** in CH_3CN is attributed to bond rupture of the bridging acetato ligand(s) and the formation of the six-coordinate monocationic acetonitrile species $[\text{Ni}_2(\mu\text{-L}^{\text{ClO}})(\mu\text{-OAc})(\text{OAc})(\text{CH}_3\text{CN})]^+$ or $[\text{Ni}_2(\mu\text{-L}^{\text{ClO}})(\text{OAc})_2(\text{CH}_3\text{CN})_2]^+$ without the release of OAc^- ion. In contrast, the value of $\Lambda_M = 280 \text{ } \Omega^{-1}\text{cm}^2\text{mol}^{-1}$ observed for $[\text{Cu}_2(\mu\text{-L}^{\text{ClO}})(\mu_2\text{-OAc})(\text{ClO}_4)](\text{ClO}_4)$ (**3**) is consistent with an 1:2 electrolyte behavior, attributed to the dissociation of the weakly bound coordinated perchlorate ligand to produce $[\text{Cu}_2(\mu\text{-L}^{\text{ClO}})(\mu_2\text{-OAc})]^{2+} + 2 \text{ClO}_4^-$. A similar conductivity trend was reported for $[\text{Cu}_2(\mu\text{-L}^{\text{ClO}})(\mu\text{-pz})(\text{ClO}_4)](\text{ClO}_4)$, where pz = pyrazole anion.^{1(b)} Four of the synthesized complexes revealed doubly bridged acetate, $[\text{M}_2(\mu\text{-L}^{\text{ClO}})(\mu_2\text{-OAc})_2]^+$ (M = Ni(II) in complexes **1** and **2**; M = Zn (II) in **5**; M = Mn(II) in **6**). With the Cu(II) complexes two different coordination modes were observed for the acetate anion: a single bridging acetate in $[\text{Cu}_2(\mu\text{-L}^{\text{ClO}})(\mu_2\text{-OAc})(\text{ClO}_4)]^+$ (**3**) and two mono-dentate acetates in $[\text{Cu}_2(\mu\text{-L}^{\text{ClO}})(\text{OAc})_2]^+$ (**4**), depending on the nature of the counter ion (see X-ray section).

Spectroscopic characterization of the complexes

The IR spectra of the complexes display some common features. Complexes **1**, **4** and **6** showed a broad absorption band over the frequency range $3430\text{-}3450 \text{ cm}^{-1}$ due to $\nu(\text{O-H})$ stretching vibration of the lattice water. The perchlorate complexes **2**, **3** and **6** displayed the $\nu(\text{Cl-O})$ band as a broad strong absorption over the region $1120\text{-}1090 \text{ cm}^{-1}$. The split of this band into two or three bands in complexes **2** and **3**, respectively is most likely due to the reduction of the ClO_4^- symmetry from T_d to C_{3v} or C_{2v} symmetries as a result of the coordination of ClO_4^- to the metal center as in complex **3** and/or to the involvement of the counter ClO_4^- ion in H-bonding with the ligand or its presence in a distorted location. The corresponding hexafluorophosphate complexes **1**, **4** and **5** showed a strong absorption band around 840 cm^{-1} due to $\nu_{\text{as}}(\text{P-F})$. The complexes also displayed a series of strong to weak intensity bands over the $1610\text{-}1440 \text{ cm}^{-1}$ region which are attributed to the pyridyl and C-O of the acetato group moieties.⁴⁰

The UV-Vis spectral data of the complexes **1-6**, recorded in CH_3CN , are summarized in Table 1. The Ni(II) complexes **1** and **2** display similar spectra with three absorption maxima located at 960, 655 and 490 nm which indicates the same coordination environment around the central Ni(II) ions. This spectral pattern is consistent with octahedral geometry around the $3d^8$

Ni(II) ion and results from the electronic d–d transitions $^3T_{2g}(F) \leftarrow ^3A_{2g}(F)$, $^3T_{1g}(F) \leftarrow ^3A_{2g}(F)$ and $^3T_{1g}(P) \leftarrow ^3A_{2g}(F)$, respectively.⁵⁴ The spectrum of copper(II) complex $[Cu_2(\mu-L^{ClO})(OAc)_2](PF_6) \cdot H_2O$ (**4**) revealed the presence of two maxima at 404 and 670 nm, assigned to the $d_{xz}, d_{yz} \rightarrow d_x^2 - y^2$ and $d_{xy} \rightarrow d_x^2 - y^2$ transitions in a distorted square pyramidal (SP) environment around the central Cu^{2+} ions.⁵⁵ The corresponding complex $[Cu_2(\mu-L^{ClO})(\mu_2-OAc)(ClO_4)](ClO_4)$ (**3**) displayed a similar spectral pattern with two maxima at 426 and a broad band around 800 nm. This is attributed to presence of a distorted trigonal bipyramidal geometry (TBP) around the central Cu^{2+} ions, $[Cu_2(\mu-L^{ClO})(\mu_2-OAc)]^{2+}$ (the weakly coordinated ClO_4^- ligand in complex **3** is dissociated in CH_3CN as indicated by the conductivity measurements).^{46(a),55,56} The electronic spectrum of $[Mn_2(L^{ClO}-O)(\mu_2-OAc)_2](ClO_4) \cdot H_2O$ (**6**) exhibits a very intense band at 316 nm with a shoulder around 500 nm (Table 1). The former band results from an M→L CT transition in a distorted octahedral environment.⁵⁴ The Zn(II) complex **5** displays a very strong maximum at 303 which is assigned to an L→M CT transition.^{54(a)}

Table 1. UV-Vis Spectroscopic and Molar Conductivity Data for **1-6** in CH_3CN .

Complex	λ_{max} (ϵ_{max} , $M^{-1}cm^{-1}$)	Λ_M ($\Omega^{-1}cm^2mol^{-1}$)
$[Ni_2(\mu-L^{ClO})(\mu_2-OAc)_2](PF_6) \cdot 3H_2O$ (1)	490 (sh), 645 (11.5), ~960 (25.6,b)	131
$[Ni_2(\mu-L^{ClO})(\mu_2-OAc)_2](ClO_6) \cdot CH_3COCH_3$ (2)	490 (sh), 644 (7.2), ~958 (22,b)	152
$[Cu_2(\mu-L^{ClO})(\mu_2-OAc)(ClO_4)](ClO_4) \cdot 2H_2O$ (3)	426 (465), ~800 (202,b)	290
$[Cu_2(\mu-L^{ClO})(OAc)_2](PF_6) \cdot H_2O$ (4)	404 (713), ~670 (155,b)	131
$[Zn_2(\mu-L^{ClO})(\mu_2-OAc)_2](PF_6)$ (5)	303 (2610)	132
$[Mn_2(L^{ClO}-O)(\mu_2-OAc)_2](ClO_4) \cdot H_2O$ (6)	316 (3550), ~500 (sh)	167

The 1H and ^{13}C NMR spectra of $[Zn_2(\mu-L^{ClO})(\mu_2-OAc)_2](PF_6)$ (**5**) were measured in deuterated dimethylsulfoxide ($DMS-d_6$) (Figures S1 and S2, respectively). The spectra did not confirm the equivalency of the two binding sites as indicated by the appearance of sixteen aromatic carbon and the corresponding nine proton resonances. This behavior indicates that the two pyridyl groups within each site are not identical. Moreover, five resonances were observed for the methylene protons of $-N-CH_2-py$ and $-N-CH_2-ph$ where each proton showed two closely related resonances over the chemical shift region $\delta = 3.69-4.41$ ppm indicating that these protons are not coupled equally. The structure of the complex cation and its atom numbering scheme is illustrated in Chart S1 (supporting information).

Crystal structures of the complexes (1-6)

Perspective views of complexes **1** - **6** together with partial atom numbering schemes are given in Fig. 1. The common features of the six complexes are dinuclear complex cations, bridged by a deprotonated O1 oxygen atom of a central 4-chloro-phenolate moiety of $L^{Cl}O^-$ (Table 2). Each M(II) center within a dinuclear complex cation is further coordinated to three N donor atoms of one bis-pyridylaminomethyl-group. Coordination number 6 with distorted octahedral geometry is completed in compounds **1**, **2**, **5** and **6** by oxygen atoms of two $\mu(O,O')$ -bridging acetate groups. The Ni-O/N, Zn-O/N and Mn-O/N bond distances are in the range 2.0097(16) – 2.1297(14), 2.005(3) – 2.228(3) and 2.0903(11) – 2.3319(12) Å, respectively. In the crystal structure of **3**, the two Cu(II) centers are further linked by one $\mu(O,O')$ -bridging acetate group. The axial site of the distorted square pyramid around the Cu1 center is occupied by O1 (τ -value = 0.20).⁵⁷ Coordination number six around the Cu2 center is completed by the O5 atom of a perchlorate anion [2.781(2) Å]. In case of **4** distorted SP geometry around each Cu(II) center is completed by O atom of terminal acetate group. Both axial sites are occupied by the bridging phenoxido oxygen atom O1 (τ -values are 0.16 and 0.17, respectively). The dinuclear complex cations co-crystallize with PF_6^-/ClO_4^- counter anions and solvent molecules (CH_3COCH_3 for **2**, water for **1** and **4**). Selected bond parameters and possible hydrogen bonds are presented in Tables S2-S8 (see supporting information section) for complexes **1-6**, respectively.

Table 2. Geometric parameters of the M-O-M bridges in the dinuclear units of **1** – **6**.

Compound	M1···M2 (Å)	M1-O1-M2 (°)	M1-O1 (Å)	M2-O1 (Å)
$[Ni_2(\mu-L^{Cl}O)(\mu_2-OAc)_2](PF_6) \cdot 3H_2O$ (1)	3.4131(5)	115.70(7)	2.0097(16)	2.0216(15)
$[Ni_2(\mu-L^{Cl}O)(\mu_2-OAc)_2](ClO_4) \cdot CH_3COCH_3$ (2)	3.4346(3)	116.43(6)	2.0209(12)	2.0198(12)
$[Cu_2(\mu-L^{Cl}O)(\mu_2-OAc)(ClO_4)](ClO_4)$ (3)	3.5711(6)	118.83(9)	2.2089(19)	1.9362(19)
$[Cu_2(\mu-L^{Cl}O)(OAc)_2](PF_6) \cdot H_2O$ (4)	3.9388(3)	128.13(7)	2.1972(14)	2.1826(14)
$[Zn_2(\mu-L^{Cl}O)(\mu_2-OAc)_2](PF_6)$ (5)	3.3935(8)	113.71(11)	2.040(2)	2.013(2)
$[Mn_2(L^{Cl}O)(\mu_2-OAc)_2](ClO_4) \cdot H_2O$ (6)	3.4515(3)	109.11(4)	2.0903(11)	2.1216(10)

Please insert Fig 1 (p-39) close to here

Magnetic properties

The experimental magnetic data of complexes **1-4** and **6** are shown in Figs 2-6, respectively. The room temperature values of the effective magnetic moments of the Ni(II) compounds ($\mu_{\text{eff}}/\mu_B = 4.41$ for **1** and 4.45 for **2**) can be compared with the expected spin-only magnetic moment $\mu_{\text{eff}} = 4.00\mu_B$ of two a system with uncoupled spins $S_1 = S_2 = 1$ ($g = 2.0$). The slightly higher experimental values are due to angular momentum contribution to the ground state from excited states. The decrease of μ_{eff}/μ_B on cooling is observed for both Ni(II) compounds, suggesting the presence of antiferromagnetic exchange, however in compound **1**, the decrease of μ_{eff}/μ_B is more pronounced with a maximum at $T_{\text{max}} = 5.4$ K in the M_{mol} vs. T curve, which demonstrates a stronger magnetic interaction in **1**. The magnetic behavior of the Cu(II) compounds is different. In case of **3**, μ_{eff}/μ_B increases upon cooling as a result of ferromagnetic exchange (Figure 4), while the μ_{eff}/μ_B of **4** is almost constant over the whole temperature range (Fig. 5). Finally, the magnetic behavior of the Mn(II) compound **6** manifests strong antiferromagnetic exchange by declination of μ_{eff}/μ_B from the theoretically expected value 8.37 ($g = 2.0$) for two uncoupled spins $S_1 = S_2 = 5/2$ even at room temperature ($\mu_{\text{eff}}/\mu_B = 7.83$ for **6**) and existence of a maximum located at $T_{\text{max}} = 35.0$ K in M_{mol} vs. T curve (Fig. 6). Since all the investigated compounds are dinuclear, the analysis of the magnetic data was based on the spin Hamiltonian for dinuclear systems of the form.⁵⁸

$$\hat{H} = -J(\vec{S}_1 \cdot \vec{S}_2) + \sum_{i=1}^2 D_i(\hat{S}_{i,z}^2 - \hat{S}_i^2 / 3) + \mu_B B g_i \hat{S}_{i,a} \quad (1)$$

where the isotropic exchange (J), zero-field splitting (D) and Zeeman term (g) are incorporated. The parameter a defines orientation of the magnetic field vector, $\mathbf{B}_a = B(\sin\theta\cos\varphi, \sin\theta\sin\varphi, \cos\theta)$. In the case of Mn(II) and Cu(II) compounds, the magnetic anisotropy was not considered, so the molar magnetization was calculated as

$$M_{\text{mol}} = N_A kT \frac{\partial \ln Z}{\partial B} \quad (2)$$

where Z is the partition function. However, a non-zero D -parameter was necessary in the analysis of Ni(II) compounds, and an integral average of molar magnetization was calculated in order to properly simulate the powder sample signal as

$$M_{\text{mol}} = 1 / 4\pi \int_0^{2\pi} \int_0^\pi M_a \sin\theta d\theta d\varphi \quad (3)$$

For all compounds under investigation, both temperature and field dependent magnetization data were fitted simultaneously. As a result, the fitted magnetic data which are

depicted by solid lines in Figs 2-6 showed good agreement with the experimental data. In Ni(II) compound **1**, the data was fitted with $J = -3.70 \text{ cm}^{-1}$, $D = +6.38 \text{ cm}^{-1}$, $g = 2.16$, $\chi_{\text{TIP}} = 4.84 \times 10^{-9} \text{ m}^3 \text{mol}^{-1}$, where χ_{TIP} is a parameter accounting for the temperature-independent paramagnetism. We have also tried to fit experimental data with a negative D -parameter but without success. In Ni(II) complex **2**, it was possible to make good fits for both negative ($J = -1.01 \text{ cm}^{-1}$, $D = -4.96 \text{ cm}^{-1}$, $g = 2.17$, $\chi_{\text{TIP}} = 4.80 \times 10^{-9} \text{ m}^3 \text{mol}^{-1}$ – Fig. 3) and positive ($J = -1.20 \text{ cm}^{-1}$, $D = +2.80 \text{ cm}^{-1}$, $g = 2.17$, $\chi_{\text{TIP}} = 4.77 \times 10^{-9} \text{ m}^3 \text{mol}^{-1}$, Fig. S3) D -parameters. Evidently, the antiferromagnetic exchange in **1** is stronger than that observed in **2**, which can be attributed to small differences in the coordination environments around the central Ni(II) ions (Table 2) as a result of different solvents of crystallization in the two complexes. The Cu(II) ions with $S = \frac{1}{2}$ do not have predisposition for zero-field splitting, therefore only isotropic exchange was taken into account. This treatment resulted in $J = +15.4 \text{ cm}^{-1}$, $g = 2.13$, $\chi_{\text{TIP}} = 6.80 \times 10^{-9} \text{ m}^3 \text{mol}^{-1}$ for **3** and $J = -0.55 \text{ cm}^{-1}$, $g = 2.12$, $\chi_{\text{TIP}} = 1.58 \times 10^{-9} \text{ m}^3 \text{mol}^{-1}$ for **4**, thus confirming the significant ferromagnetic exchange in **3** and almost negligible antiferromagnetic exchange in **4**. The magnetic data for the dinuclear Mn(II) complex **6** was treated with presumption that $D \approx 0 \text{ cm}^{-1}$, because a large antiferromagnetic exchange results in an $S = 0$ ground state, which does not bear any information about D , and excited states with $S > 0$ are too high in energy to be used for the identification of magnetic anisotropy. As a result, the following spin Hamiltonian parameters were obtained for **6**: $J = -9.40 \text{ cm}^{-1}$, $g = 2.01$, $\chi_{\text{PI}} = 0.67\%$, where χ_{PI} is molar fraction of mononuclear paramagnetic impurity.

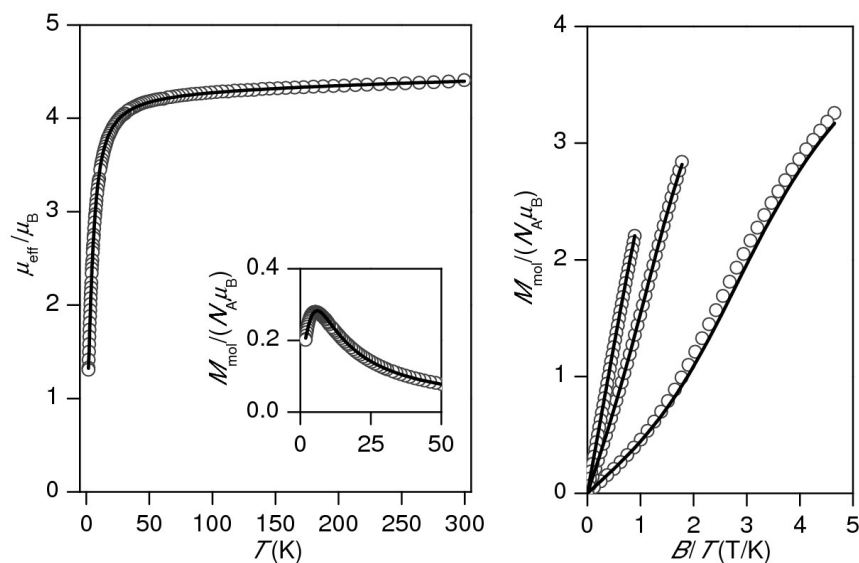


Fig. 2. Magnetic data for **1**. *Left*: temperature dependence of the effective magnetic moment and molar magnetization measured at $B = 1$ T. *Right*: isothermal magnetizations measured at $T = 2, 5$ and 10 K. Open circles: experimental data, solid lines: calculated data using equation 1, with $J = -3.70 \text{ cm}^{-1}$, $D = +6.38 \text{ cm}^{-1}$, $g = 2.16$, $\chi_{\text{TIP}} = 4.84 \times 10^{-9} \text{ m}^3 \text{ mol}^{-1}$.

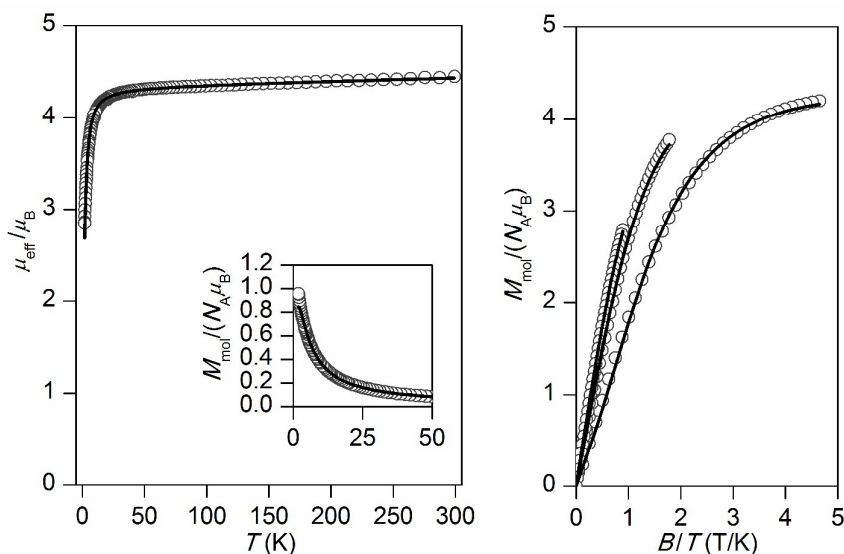


Fig. 3. Magnetic data for **2**. *Left*: temperature dependence of the effective magnetic moment and molar magnetization measured at $B = 1$ T. *Right*: isothermal magnetizations measured at $T = 2, 5$ and 10 K. Open circles: experimental data, solid lines: calculated data using equation 1, with $J = -1.01 \text{ cm}^{-1}$, $D = -4.96 \text{ cm}^{-1}$, $g = 2.17$, $\chi_{\text{TIP}} = 4.80 \times 10^{-9} \text{ m}^3 \text{ mol}^{-1}$.

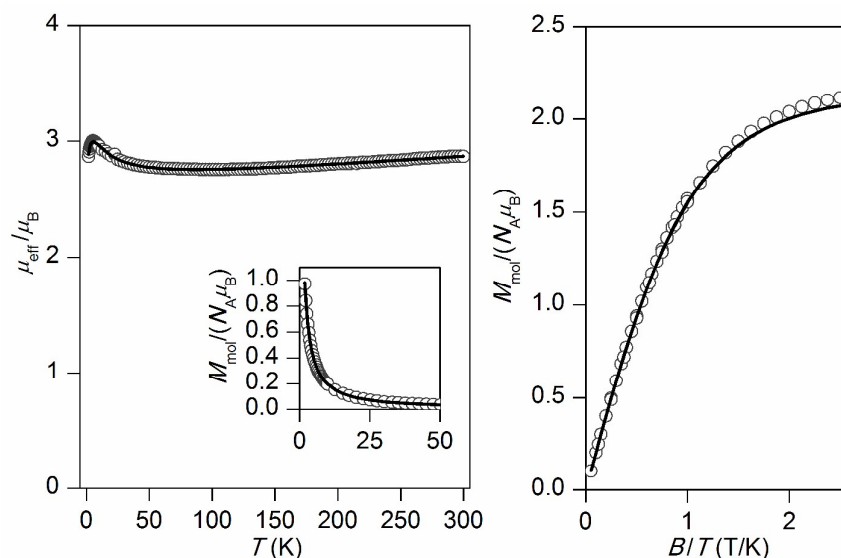


Fig. 4. Magnetic data for **3**. *Left*: temperature dependence of the effective magnetic moment and molar magnetization measured at $B = 1$ T. *Right*: isothermal magnetizations measured at $T = 2$ and 5 K. Open circles: experimental data, solid lines: calculated data using equation 1, with $J = +15.4 \text{ cm}^{-1}$, $g = 2.13$, $\chi_{\text{TIP}} = 6.80 \times 10^{-9} \text{ m}^3 \text{ mol}^{-1}$.

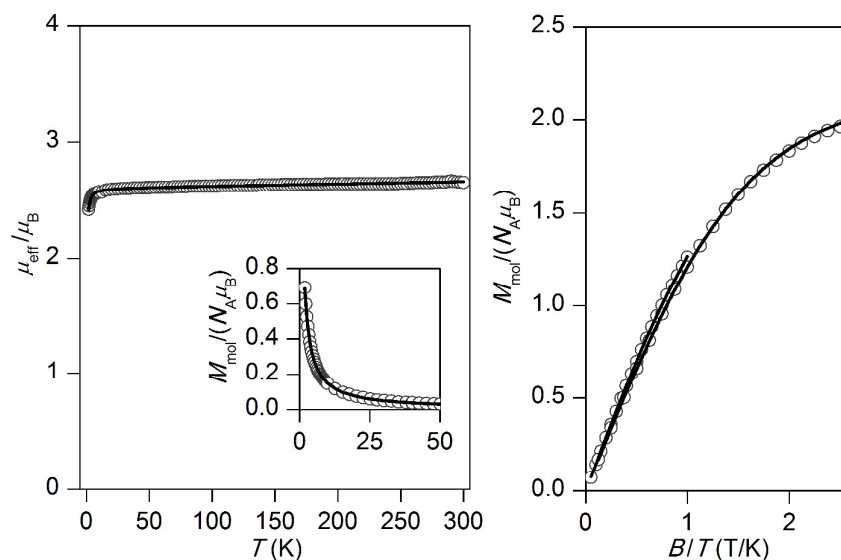


Fig. 5. Magnetic data for **4**. *Left*: temperature dependence of the effective magnetic moment and molar magnetization measured at $B = 1$ T. *Right*: isothermal magnetizations measured at $T = 2$ and 5 K. Open circles: experimental data, solid lines: calculated data using equation 1, with $J = -0.55 \text{ cm}^{-1}$, $g = 2.12$, $\chi_{\text{TIP}} = 1.58 \times 10^{-9} \text{ m}^3 \text{ mol}^{-1}$.

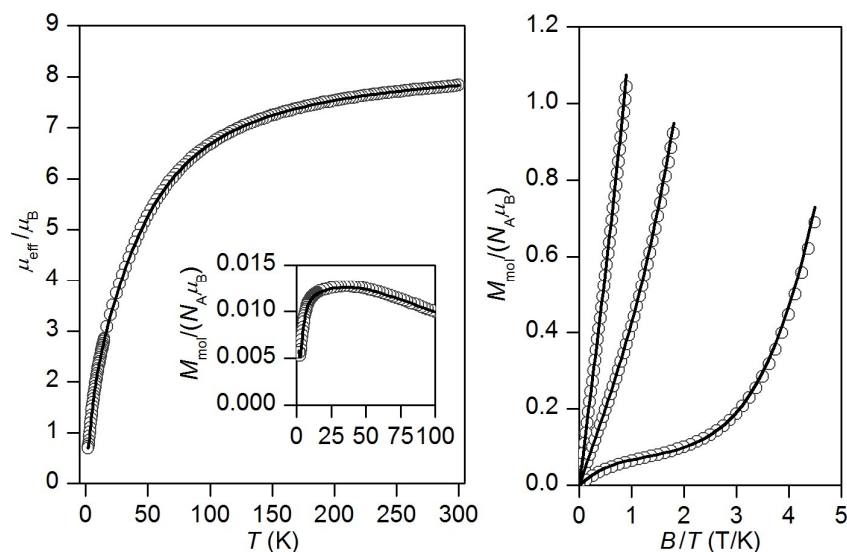


Fig. 6. Magnetic data for **6**. *Left*: temperature dependence of the effective magnetic moment and molar magnetization measured at $B = 0.1$ T. *Right*: isothermal magnetizations measured at $T = 2, 5$ and 10 K. Open circles: experimental data, solid lines: calculated data using equation 1 with $J = -9.40 \text{ cm}^{-1}$, $g = 2.01$, $x_{\text{PI}} = 0.67\%$.

DFT calculations

Our recent studies on a series of dinuclear doubly bridged Cu(II) complexes of 2,6-bis[bis(2-pyridylmethyl)aminomethyl]-4-chlorophenol ($\text{L}^{\text{Cl}}\text{-OH}$) and various bridging ligands (OH^- , $\text{O}_2\text{P}(\text{OC}_6\text{H}_5)_2^-$, $\text{C}_3\text{H}_3\text{N}_2^-$) showed that the DFT calculations of the isotropic exchange parameters J based on the B3LYP hybrid functional are helpful in understanding the efficiency of magnetic super-exchange pathways in these complexes.^{1(b)} Therefore, the exchange mechanisms for the complexes under investigation were studied using the same functional.^{1(b)} The calculations were performed on the molecular cations $[\text{Ni}_2(\mu\text{-L}^{\text{Cl}}\text{O})(\mu_2\text{-OAc})_2]^+$ **1** and **2**, $[\text{Cu}_2(\mu_2\text{-L}^{\text{Cl}}\text{O})(\mu\text{-OAc})(\text{ClO}_4)]^+$ **3**, $[\text{Cu}_2(\mu\text{-L}^{\text{Cl}}\text{O})(\text{OAc})_2]^+$ **4** and $[\text{Mn}_2(\mu\text{-L}^{\text{Cl}}\text{O})(\mu_2\text{-OAc})_2]^+$ **6** by the aid of the well-established ORCA 3.0 computational package using the def2-TZVP(-f) basis set. The J -values were evaluated from the energy difference Δ , between the high spin (HS) and broken-symmetry (BS) states

$$\Delta = E_{\text{BS}} - E_{\text{HS}} \quad (4)$$

by both Ruiz's approach⁵⁹

$$J^{\text{Ruiz}} = 2\Delta / [(S_1 + S_2)(S_1 + S_2 + 1)] \quad (5)$$

and Yamaguchi's approach⁶⁰

$$J^{\text{Yam}} = 2\Delta / \left[\langle S^2 \rangle_{\text{HS}} - \langle S^2 \rangle_{\text{BS}} \right] \quad (6)$$

where, the following spin Hamiltonian for the dinuclear system was used

$$\hat{H} = -J(\vec{S}_1 \cdot \vec{S}_2) \quad (7)$$

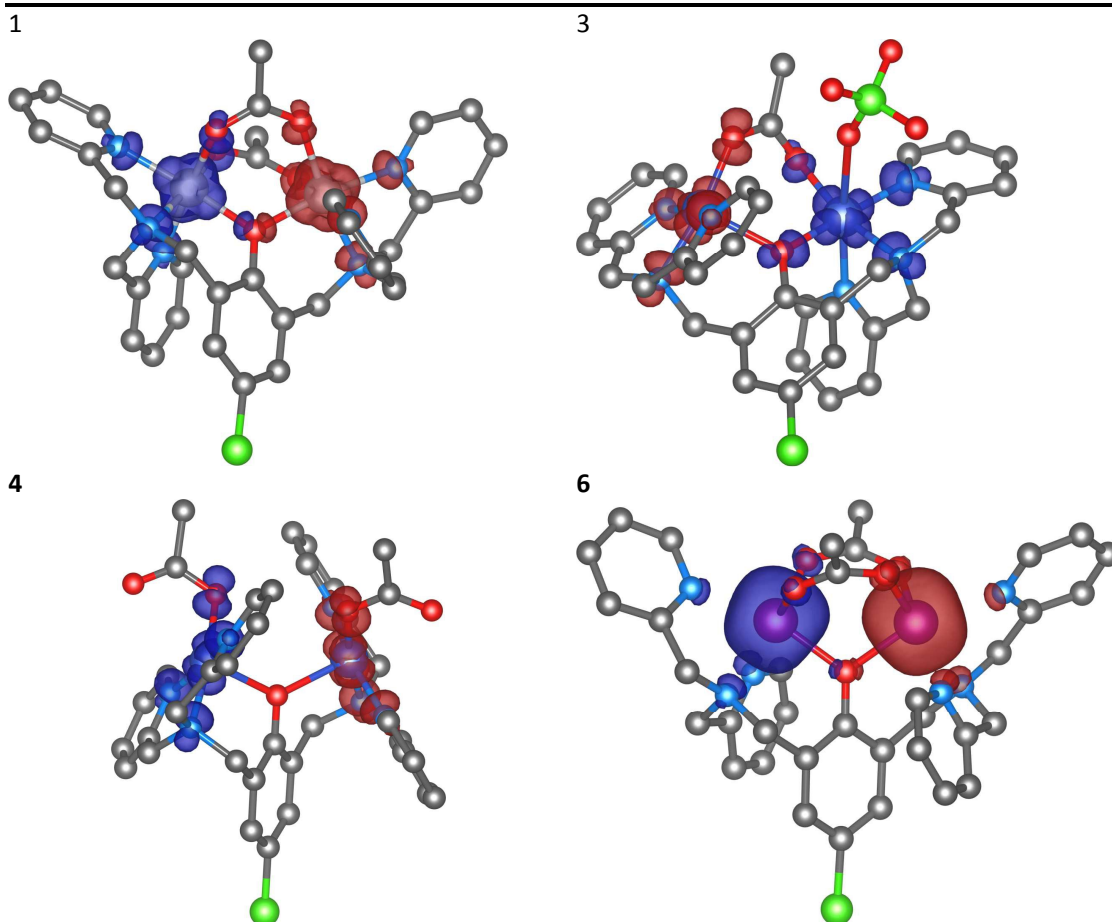


Fig. 7. Calculated isodensity surfaces of the broken symmetry spin states for molecular fragments $[\text{Ni}_2(\mu\text{-L}^{\text{ClO}})(\mu_2\text{-OAc})_2]^+$ of **1**, $[\text{Cu}_2(\mu\text{-L}^{\text{ClO}})(\mu_2\text{-OAc})(\text{ClO}_4)]^+$ of **3**, $[\text{Cu}_2(\mu\text{-L}^{\text{ClO}})(\text{OAc})_2]^+$ of **4** and $[\text{Mn}_2(\mu\text{-L}^{\text{ClO}})(\mu_2\text{-OAc})_2]^+$ of **6** using B3LYP/def2-TZVP(-f). Positive and negative spin densities are represented by dark blue, and dark red surfaces, respectively. The isodensity surfaces are plotted with the cut-off values of $0.005 \text{ e}a_0^{-3}$. Hydrogen atoms are omitted for clarity.

The results of the DFT calculations are summarized in Table 3 and the calculated spin densities for the selected compounds are depicted in Fig. 7. In all cases, the DFT calculations

resulted in J values ($J^{\text{Ruiz}}/J^{\text{Yam}}$) close to parameters extracted from the experimental magnetic data (J^{mag}), except for the copper(II) complexes **3** (Cu(II) ions adopt different geometries, square pyramidal for Cu(1) and octahedral for Cu(2)), and **4** (the two Cu(II) ions adopt the square pyramidal geometries), where the calculations were slightly overestimating the antiferromagnetic exchange (Table 3). The non-orthogonal magnetic orbitals of the broken symmetry solution with the highest overlap $S_{\alpha\beta}$ for the three compounds **1**, **3** and **6** are shown in Fig. 8. In the case of the singly bridged-phenoxido Cu(II) complex **4** where SP geometries were adopted, the unpaired electrons reside in $d_{x^2-y^2}$ orbitals, where these magnetic orbitals are well isolated and hence the magnetic interaction is almost negligible. However, the magnetic orbitals in compound **3** are close enough and at the same time they are orthogonal, which explains the observed ferromagnetic interaction in this complex (Fig. 8). The nickel(II) complexes are octahedral with the unpaired electrons in d_{z^2} and $d_{x^2-y^2}$ orbitals, and to a large extent, the spin density is delocalized on all donor atoms. The super-exchange pathway should be efficient through the phenoxido and acetato ligands, but the largest overlap was observed through the phenoxido-bridge (Fig. 8). In Mn(II) complex **6**, where all d-orbitals contain unpaired electrons, a smaller extent of spin delocalization is observed. Surprisingly, the magnetic orbitals with the highest overlap are located outside the metal-donor bonds (Fig. 8).

Table 3. DFT-calculated Net Mulliken Spin Densities (ρ), Expected Values $\langle S^2 \rangle$, Overlap $S_{\alpha\beta}$ Between the Corresponding Orbitals and Isotropic Exchange Parameters (J) from High-spin (HS) and Broken Symmetry (BS) States, Compared with the Experimental Exchange Parameters, of the Dinuclear Complexes $[\text{Ni}_2(\mu\text{-L}^{\text{ClO}})(\mu_2\text{-OAc})_2]^+$ **1** and **2**, $[\text{Cu}_2(\mu\text{-L}^{\text{ClO}})(\mu_2\text{-OAc})(\text{ClO}_4)]^+$ **3**, $[\text{Cu}_2(\mu\text{-L}^{\text{ClO}})(\text{OAc})_2]^+$ **4** and $[\text{Mn}_2(\mu_2\text{-L}^{\text{ClO}})(\mu_2\text{-OAc})_2]^+$ **6** Using the B3LYP Functional and Experimental Structural Parameters.

	1	2	3	4	6
$\rho^{\text{HS}}(\text{M1})/\rho^{\text{HS}}(\text{M2})$	1.65/1.65	1.65/1.65	0.61/0.64	0.62/0.62	4.85/4.85
$\rho^{\text{BS}}(\text{M1})/\rho^{\text{BS}}(\text{M2})$	-1.64/1.64	-1.65/1.65	-0.61/0.64	-0.62/0.62	-4.85/4.85
$\langle S^2_{\text{HS}} \rangle / \langle S^2_{\text{BS}} \rangle$	6.01/2.01	6.01/2.01	2.01/1.00	2.01/1.01	30.01/5.00
$S_{\alpha\beta}$	0.04841 0.03511	0.04388 0.03374	0.02459	0.00468	0.07766 0.04656 0.02303 0.01745 0.00813
Δ/cm^{-1}	-16.514	-7.701	+12.066	-0.279	-195.733
$J^{\text{Ruiz}}/J^{\text{Yam}} (\text{cm}^{-1})$	-5.50/-8.25	-2.57/-3.85	+12.1/+24.1	-0.279/-0.558	-13.0/-15.7
$J^{\text{mag}}/\text{cm}^{-1}$	-3.70	-1.01/-1.20	+15.4	-0.55	-9.40
$\langle \text{M-O}_{\text{Ph}}\text{-M} \rangle^\circ$	115.70	116.43	118.83	128.14	109.11
$d(\text{M-M})/10^{-10} \text{ m}$	3.413	3.435	3.571	3.939	3.452

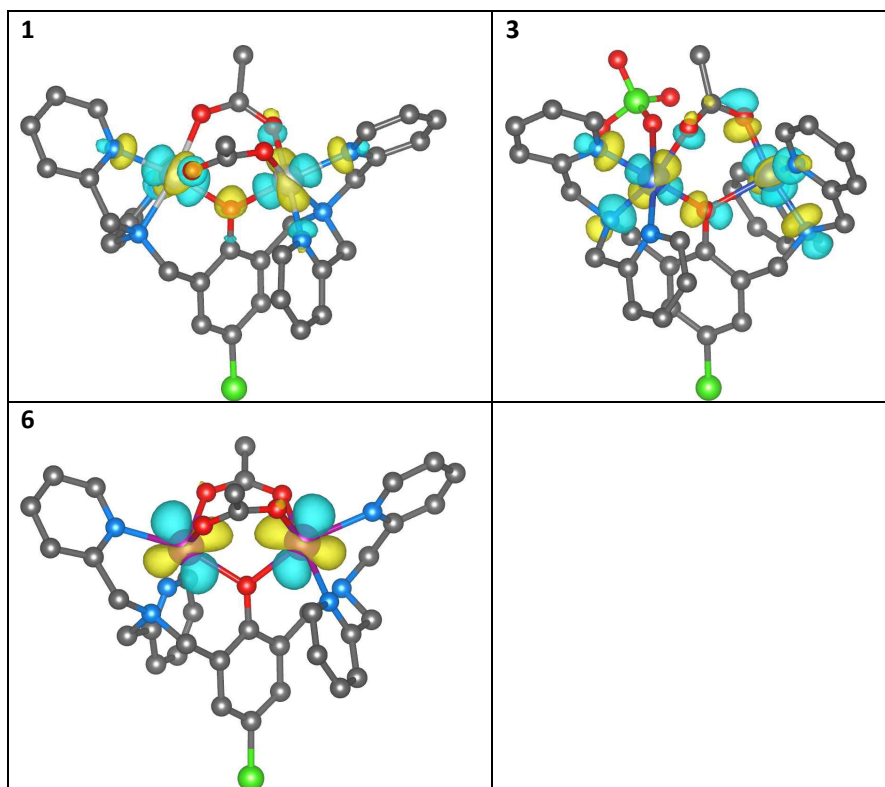


Fig. 8. The non-orthogonal magnetic orbitals with highest overlap $S_{\alpha\beta}$ of the broken-symmetry spin state visualized for $[\text{Ni}_2(\mu\text{-L}^{\text{ClO}})(\mu_2\text{-OAc})_2]^+$ of **1**, $[\text{Cu}_2(\mu\text{-L}^{\text{ClO}})(\mu_2\text{-OAc})(\text{ClO}_4)]^+$ of **3** and $[\text{Mn}_2(\mu\text{-L}^{\text{ClO}})(\mu_2\text{-OAc})_2]^+$ of **6**. Hydrogen atoms are omitted for clarity.

Interactions of metal complexes with DNA

Some copper(II), zinc(II), nickel(II) and cobalt(II) complexes have been reported to serve as efficient artificial nucleases for DNA cleavage.^{25,33-36,39,47,56} In general, it is well established that the supercoiled circular form of plasmid ds-DNA (SC-form) is cleaved to the relaxed open circular form of DNA (OC-form), which upon further cleavage results in the formation of the linear DNA (L-form). In this work, the interaction of the dinuclear complexes **1-5** with DNA has been investigated under the physiological conditions. The interaction of the copper(II) (**3** and **4**) and zinc(II) (**5**) complexes with DNA did not show any nuclease activity as clearly illustrated in Figs 9 and 10, respectively. Also, it emerges that the concentration of the SC-form of plasmid DNA was decreased without showing any sign of increase neither of the OC-form nor the linear L-form. On the other hand, the observed effect is not augmented by longer incubation of plasmid DNA with these complexes. As a model molecule, copper(II) complex **3** was examined at longer incubation

time and at different complex concentrations. The gel electrophoretic band pattern remained the same even if the interaction time was prolonged up to 22 hours (Fig. S4). The observed effects might be explained by direct competition of these complexes with the ethidium bromide (EtBr) which was used in the gel electrophoresis; no damaging/cleavage of DNA was noticed neither after long reaction time nor at high complex concentrations. Replacing the intercalated EtBr from its binding sites on DNA by zinc(II) or copper(II) complexes could lead to the reduction of EtBr fluorescence on the gel as it has been seen from the decrease of intensities of the individual bands.

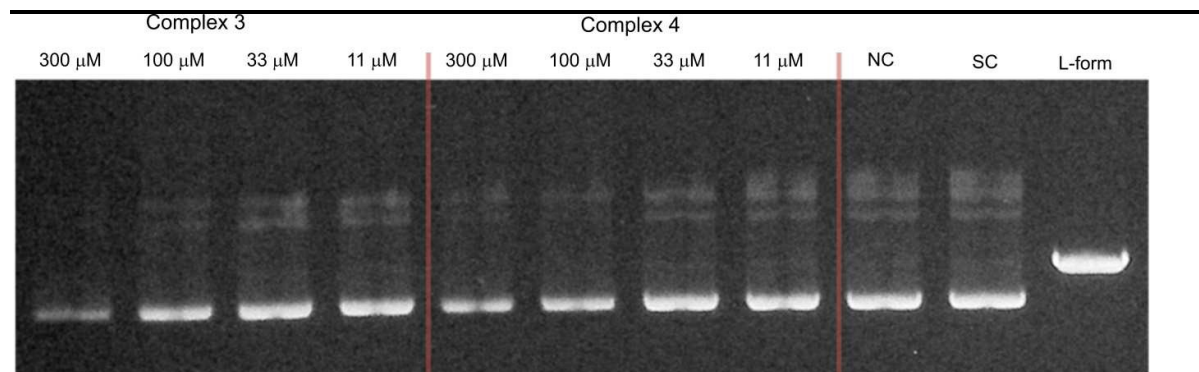


Fig. 9. Agarose gel (in TBE buffer with pH 8.4 at room temperature) electrophoresis patterns for the effect of concentrations of Cu(II) complexes **3** (*left*) and **4** (*middle*) (11–300 μ M) on the native pUC19 plasmid DNA [the calculated concentration of base pairs (bp) = 23 μ M]. NC is the negative control, SC the supercoiled plasmid DNA, and L-form represents the sample of native plasmid linearized by *Hind*III endonuclease.

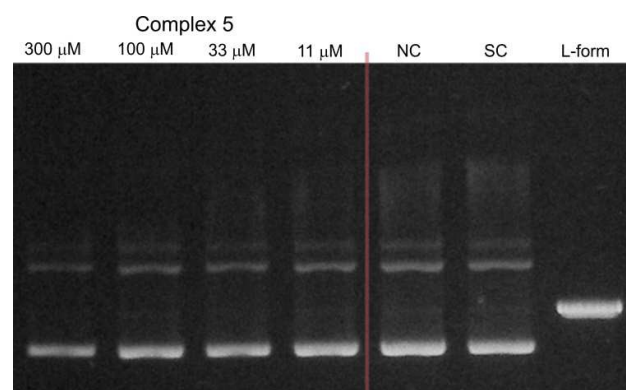


Fig. 10. Agarose gel (in TBE buffer with pH 8.4 at room temperature) electrophoresis patterns for the effect of concentrations of Zn(II) complex **5** (*left*) (11, 33, 100 and 300 μ M) on the native pUC19 plasmid DNA [the calculated concentration of base pairs (bp) = 23 μ M]. NC is the negative control, SC the supercoiled plasmid DNA, and L-form represents the sample of native plasmid linearized by *Hind*III endonuclease.

The catalytic activity of DNA was also conducted in the presence of Ni(II) complexes **1** and **2** in a similar fashion as that described for complexes **3-5**. The results which are depicted by the gel electrophoresis in Figure 11 showed that no nuclease activity was observed with the two complexes. However, unlike the copper(II) (**3** and **4**) and zinc(II) (**5**) complexes, the nickel(II) complexes $[\text{Ni}_2(\mu\text{-L}^{\text{ClO}})(\mu_2\text{-OAc})_2](\text{PF}_6)\cdot 3\text{H}_2\text{O}$ (**1**) and $[\text{Ni}_2(\mu\text{-L}^{\text{ClO}})(\mu_2\text{-OAc})_2](\text{ClO}_4)\cdot \text{CH}_3\text{COCH}_3$ (**2**) revealed a strong ability to unwind the supercoiled plasmid dsDNA and behave as intercalators. Unwinded and partially unwinded plasmid conformations were observed in the plasmid-DNA gel electrophoresis as a “smear” (Fig. 11). A similar trend was recently reported by A. Terenzi et al. in the interaction of Ni(II)-salphen complex (salphen = the anion of *N,N*-bis-salicylidene-1,2-phenylenediamine) with native DNA.⁴⁸ In addition, the unwinding activity by the two nickel(II) complexes **1** and **2** was associated by a “smear” of DNA molecules which is slower than that detected for the OC-form. Perhaps, this could be caused either by the neutralization of the negative charge of DNA or due to cross-linking of the DNA molecules or a combination of both effects which led to an increase in their molecular weights and hence changes in the conformations. The dependence of the total amounts of the plasmid SC-form as a function of the concentration of the complexes **1-5** is shown in Fig. 12.

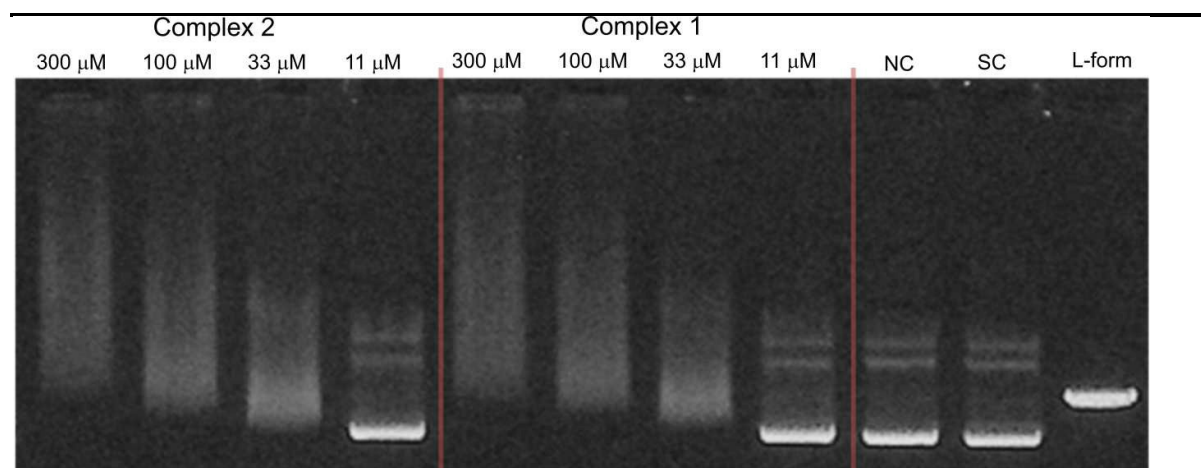


Fig. 11. Agarose gel (in TBE buffer with pH 8.4 at room temperature) electrophoresis patterns of the interaction of Ni(II) complexes **2** (*left*) and **1** (*middle*) at different concentrations (11-300 μM) with the native pUC19 plasmid [the calculated concentration of base pairs (bp) = 23 μM], where NC is to the negative control, SC is the supercoiled plasmid DNA, and L-form represents the sample of native plasmid linearized by *Hind*III endonuclease.

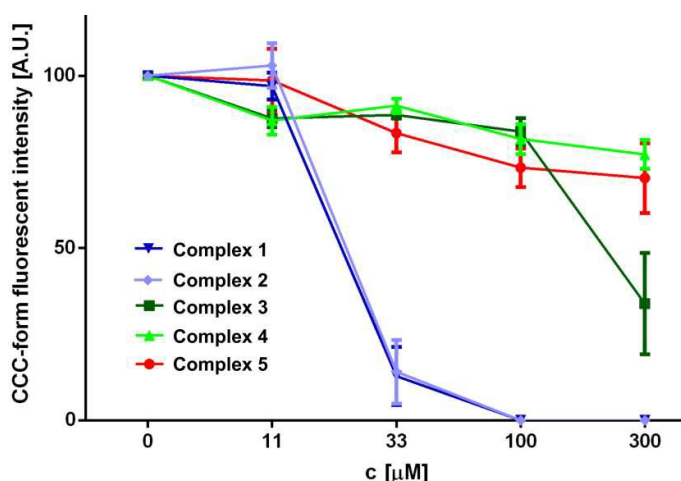


Fig. 12. The graphical interpretation of the concentration-dependent decline in the portion of the supercoiled plasmid DNA (also referred to as SC-form) in the samples showing the effective interaction of Ni(II) complexes with plasmid DNA leading to the formation of interconnected multiplexes or decrease of the surface charge of the polynucleotide backbone (or a combination of both). Other complexes showed the ability to quench the fluorescence of ethidium bromide–plasmid DNA complex, which is evident from the linear dependence of the decreasing fluorescence of the SC-form with the increasing concentration of the applied transition metal complex.

In order to understand the mechanistic pathway responsible for the attenuation of the supercoiled plasmid DNA observed in the fluorescence electrophoreograms for the Ni(II) complexes **1** and **2**, the interaction of the Ni(II) complexes was performed in the presence of oxidative scavengers (DMSO and KI), the metal competitor MgSO_4 , and the metal chelator EDTA (the complex/inhibitor molar ratio is 1:1).^{38,39,46} Therefore, a series of experiments for DNA–Ni(II) interaction were conducted at two different Ni(II) concentrations (33 and 300 μM) in the presence of these inhibitors (DMSO, KI, MgSO_4 and EDTA) and the results are illustrated in Figures 13 and 14. Inspection of these figures demonstrates that MgSO_4 , DMSO and KI had no effect for the complexes on the DNA structure. However, in case of complex **2**, EDTA was able to attenuate the unwinding of supercoiled plasmid DNA (Figs 14 and 15) at low complex concentration (33 μM). These results are quantified in Fig. 15 which indicates that nickel(II) ion is important for the plasmid DNA unwinding, where the bond between the complexes **1** and **2** with DNA is stronger than that of Ni(II)–EDTA.

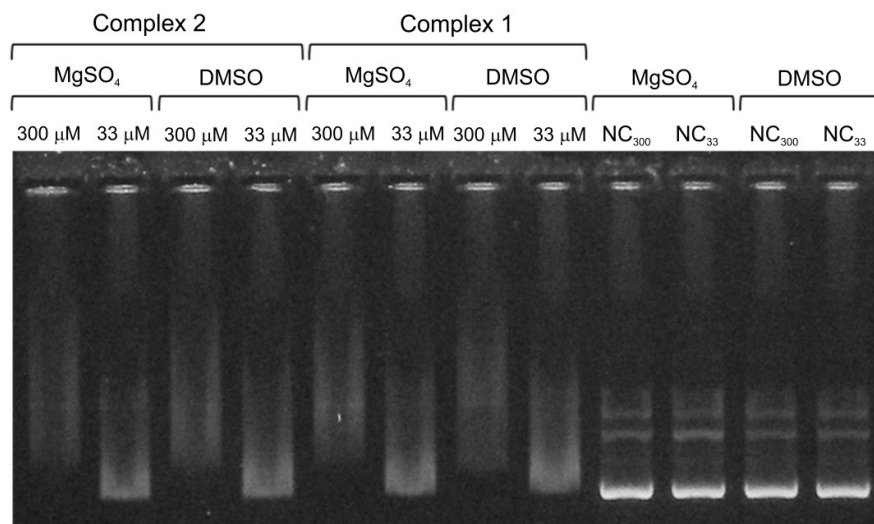


Fig.13. The electrophoreogram showing the effect of the addition of hydroxyl scavenger DMSO and increased ionic strength on the interactions of Ni(II) complexes **2** and **1** with plasmid DNA. NC is the negative control with the appropriate concentration of additional substance. The indicated concentration levels represent both the concentrations of applied complexes, as well as the concentration of added substances (molar ratio 1:1).

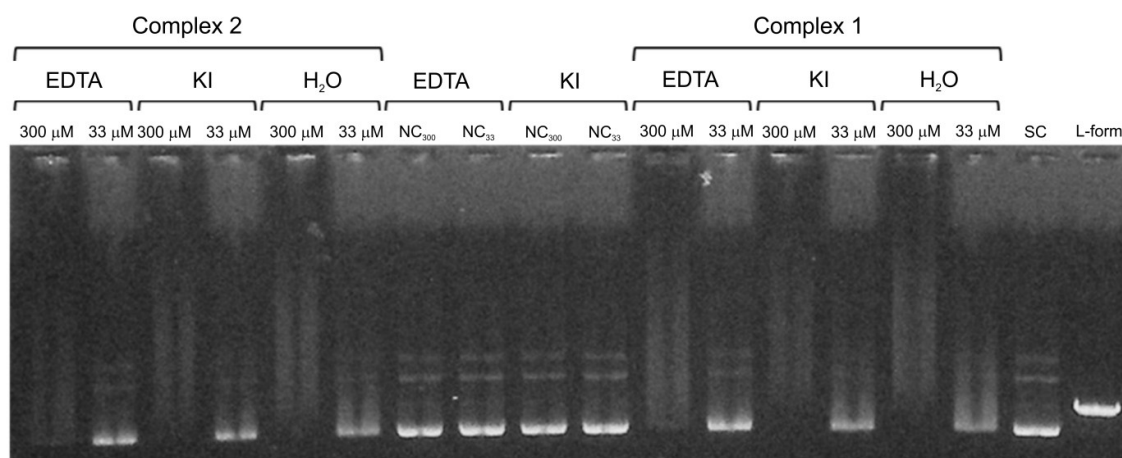


Fig. 14. The electrophoreogram showing the effect of addition of different inhibitors (and H₂O as a positive control) on the interactions of the Ni(II) complexes **2** and **1** with plasmid DNA. NC is the negative control with the appropriate concentration of additional substance. The indicated concentration levels represent both the concentrations of applied complexes, as well as the concentration of added substances (molar ratio 1:1).

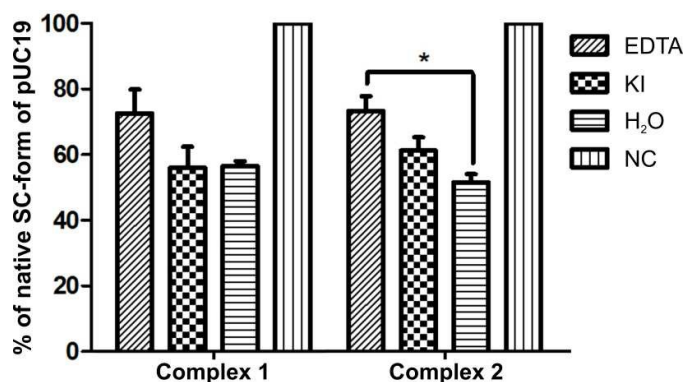


Fig. 15. The diagram shows the effect of different inhibitors on the decline in the portion of the supercoiled plasmid DNA (also referred to as SC-form) in the samples showing the effective interaction of the Ni(II) complexes **1** and **2** with plasmid DNA (at the 33 μM concentration level, leading to the formation of interconnected multiplexes). The importance of transition metal function in the formation of the mentioned superstructures was confirmed as the portion of the SC-form of plasmid DNA in the group with added EDTA at 33 μM level differs significantly from the positive control ($p < 0.05$).

Phosphodiester hydrolysis

The phosphatase reactivity of complexes **1**, **3**, and **5** was probed with a well-established spectroscopic assay using the activated phosphodiester BDNPP as a model substrate.^{21,61-63} Cleavage of the P-O bond was followed at 25° C by monitoring the hydrolysis product 2,4-dinitrophenolate by its strong absorption at 400 nm ($\epsilon = 12,000 \text{ M}^{-1}\text{cm}^{-1}$).⁶³ All measurements were carried out in 1:1 acetonitrile-buffer mixtures. The pH dependence of the activity was studied by varying the pH of the multicomponent buffer (pH 5.5 – pH 10.5) in the assay; the plots obtained for the complexes **1** and **5** are presented in Fig. 16. Complex **3** did not show a significant increase of the BDNPP hydrolysis rate. The data were fitted to equation 8, which is based on a model for a diprotic system with two active species.⁶⁴

$$v_0 = \frac{v_{\max} \left(1 + \frac{\gamma K_{a2}}{[H^+]} \right)}{\left(1 + \frac{[H^+]}{K_{a1}} + \frac{K_{a2}}{[H^+]} \right)} \quad (8)$$

Here, v_0 and is the initial rate and v_{\max} is the maximum reaction rate that is reached under given conditions. The factor γ is related to the relative activity of the two active species in equilibrium (E^nS and $E^{n-1}S$); a value of γ less than unity corresponds to a more active E^nS adduct and a value

higher than one considers the deprotonated adduct $E^{n-1}S$ as more active.^{64,65} The resulting pK_a and γ values are listed in Table 4.

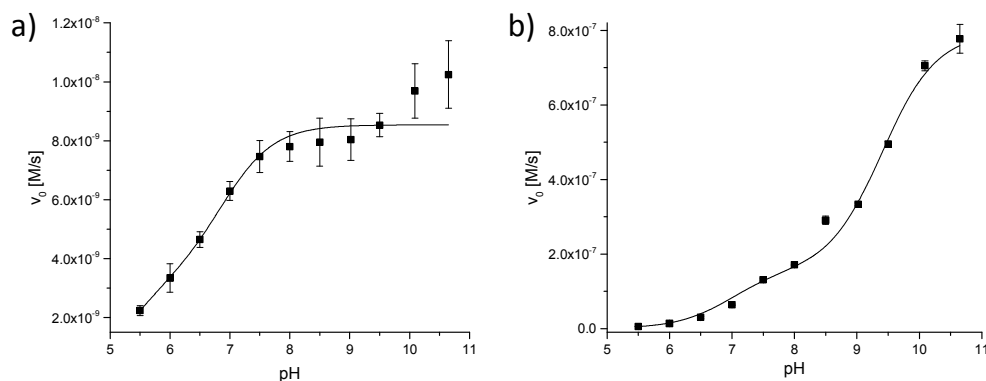


Fig. 16. pH dependence of the BDNPP (2.5 mM) hydrolysis activity by complexes (0.02 mM) a) **5**, and b) **1** (the pH values refer to the aqueous component).

Table 4. Kinetic data: k_{cat} in ($10^{-3} s^{-1}$), K_M in (mM) and k_{cat}/K_M in ($s^{-1} M^{-1}$) of the BDNPP hydrolysis (all kinetic studies were done in a mixture of acetonitrile:aqueous buffer = 1:1)^a.

Complex	$pK_a(I)$	$pK_a(II)$	γ	pH ^b	k_{cat} ($10^{-3} \cdot s^{-1}$)	K_M (mM)	k_{cat}/K_M ($10^{-3} \cdot s^{-1} mM^{-1}$)
5	5.30 ± 0.60	6.90 ± 0.31	2.52 ± 0.80	7	0.48 ± 0.05	2.55 ± 0.66	0.19 ± 0.28
				10.5	8.24 ± 2.35	54.28 ± 16.90	0.15 ± 0.42
1	6.97 ± 0.07	9.41 ± 0.22	5.03 ± 0.74	7	2.80 ± 0.13	0.21 ± 0.11	13.33 ± 0.56
				10.5	64.71 ± 0.81	2.81 ± 0.08	23.03 ± 0.03

^a The pH values refer to the aqueous component; the pH of a 1:1 mixture of buffer and acetonitrile is the same within the error as in an aqueous solution of the buffer.⁶⁶

^b pH of aqueous buffer solution used for substrate dependence assays (Michaelis-Menten measurements).

The initial rate vs. pH profiles for complexes **1** and **5** showed different shapes. The curve shape of the nickel(II) complex **1** indicates that three different complex species are present in the pH range of importance. An active species is generated in a first deprotonation step ($pK_a = 6.97$); the second deprotonation step ($pK_a = 9.41$) increases its activity further. This behavior is different from that for the zinc(II) complex **5**, which showed only a slight increase in reactivity over the pH range from 9 to 10.

The dependence of the BDNPP hydrolysis rate of complexes **1** and **5** on the substrate concentration was determined at pH 7 and pH 10.5 (Figs 17 and 18). Fitting the resulting data to the Michaelis-Menten equation provides values for the parameters k_{cat} and K_M , which are listed in

Table 4 (the catalytic efficiencies $k_{\text{cat}}/K_{\text{M}}$ have also been determined but the corresponding standard deviations do not allow a meaningful interpretation in all cases). Comparison of the two complexes allows an assessment of the impact of the metal center of the catalyst. The zinc(II) complex **5** shows lower hydrolysis rates compared to the nickel(II) complex (**1**) at pH 7 and pH 10.5. Moreover, the substrate affinity of **1** is also higher than that for **5** for both pH values investigated, resulting in higher catalytic efficiencies. Therefore, the catalytic activity of the complexes are found to decrease in the order: Ni(II) > Zn(II) > Cu(II). This order contrasts the published results for the phosphomonoester hydrolysis activities of dinuclear copper(II), zinc(II) and nickel(II) complexes of a macrocyclic ligand.⁶⁷

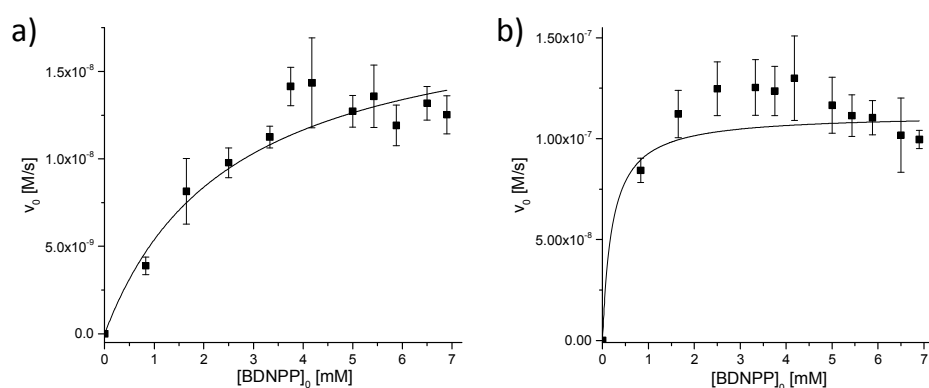


Fig. 17. Substrate concentration dependence of the BDNPP hydrolysis activity by complexes (0.04 mM; pH = 7) a) **5**, and b) **1**.

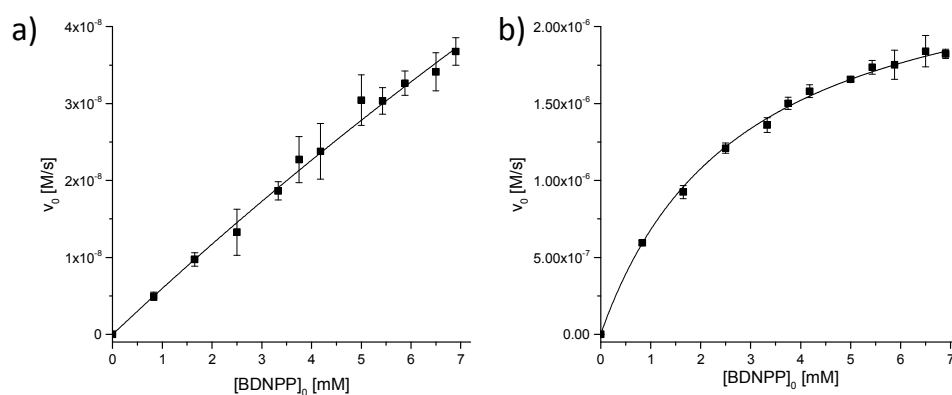
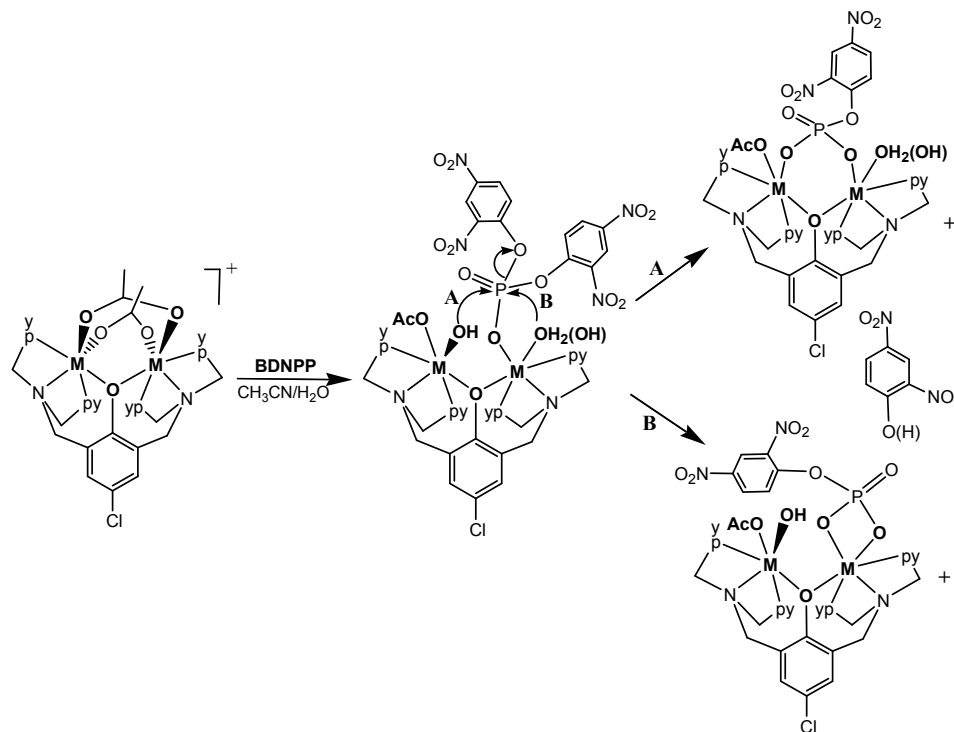


Fig. 18. Substrate concentration dependence of the BDNPP hydrolysis activity by complexes (0.04 mM; pH = 10.5) a) **5**, and b) **1**.

To account for the two observed reactive species, we can propose that in aqueous acetonitrile and in the presence of BDNPP, the doubly bridged diacetato complex $[M_2(\mu-L^{Cl}O)(\mu_2-OAc)_2]^+$ one acetate is displaced of one of the acetato groups by BDNPP and two water molecules, one coordinated to each metal ion; $[M_2(\mu-L^{Cl}O)(OAc)(H_2O)_2(BDNPP)]^+$ (Scheme 1). At neutral pH region ($pK_{a1} = 6.97 \pm 0.07$ and 5.3 ± 0.60 for complexes **1** and **5**, respectively), a hydroxo intermediate $[M_2(\mu-L^{Cl}O)(OAc)(OH)(H_2O)(BDNPP)]$ is considered to be the predominant species in solution, where the coordinated *cis*-hydroxo group attacks in an intramolecular nucleophilic reaction the phosphorous atom of the mono-coordinated BDNPP, leading to the hydrolysis of BDNPP and the formation of the product with a bridged-mono-phosphatoester (path **A** in Scheme 1). A similar dinuclear complex with a bridging μ_2 -phenylphosphate was isolated and structurally characterized with Cu(II).^{1(b)} In basic medium ($pK_{a2} = 9.41 \pm 0.22$ and 6.90 ± 0.31 for **1** and **5**, respectively), the second predominant hydroxido species in which the hydroxide and BDNPP are coordinated to the same metal center undergoes a similar hydrolytic process, resulting in the generation of 2,4-dinitrophenolate and the four-membered chelated monophosphatoester (path **B**).



Scheme 1. A tentative mechanism for the hydrolysis of BDNPP by the dinuclear metal(II) complexes ($M = Ni(II)$ or $Zn(II)$) around the neutral pH region in 1:1 acetonitrile-buffer mixtures.

The turn over numbers (TONs) of complexes **1**, **3**, and **5** were also investigated. The studies were conducted at pH 7 at room temperature and samples were taken from the assays at various intervals during the studies, diluted with solvent, and their UV-Vis spectra recorded to determine the amount of phosphoester hydrolysis. The increase in the absorbance at 400 nm, associated to the hydrolysis product 2,4-dinitrophenolate, was monitored over time and TON values calculated after eight days. The resulting data are given in Table 5.

Table 5. TON of the BDNPP hydrolysis at pH 7 with complexes **1**, **3** and **5**.

Complex	TON after 5 days	TON after 8 days
3	1 ± 1	--
1	66 ± 1	79 ± 1
5	14 ± 1	16 ± 1

In accordance with the kinetic studies the nickel(II) complex shows the highest TON and the TONs follow the order: Cu(II) < Zn(II) < Ni(II). This behavior is in contrast to two principles: a) the exchange rates of metal-coordinated water molecules increase in the order Ni(II) < Zn(II) < Cu(II), and b) the acidity of the coordinated water molecules mainly depends on the electronegativity of the metal ions, as the metal ions considered have the same charge. The electronegativities follow the order: Zn < Cu ~ Ni.⁶⁷ For these reasons, we believe that the coordination geometry of the metal ions has a significant influence on the reactivity of the complexes. An interesting observation therefore is that the two Cu(II) ions in **3** are five- and six-coordinate, respectively, whereas both Ni(II) ions in **1** and both Zn(II) ions in **5** are six-coordinate..

Experimental

Materials and Physical Measurements

Bis(2-pyridylmethyl)amine (DPA) was purchased from TCI-America. All other chemicals were commercially available and used without further purification. 2,6-Bis[bis(2-pyridylmethyl)aminomethyl]-4-chlorophenol (L^{Cl}-OH) was synthesized and characterized as recently described.^{1(a)} Infrared spectra were recorded on a JASCO FTIR-480 plus spectrometer as KBr pellets. Electronic spectra were recorded using an Agilent 8453 HP diode array UV-Vis spectrophotometer. ¹H and ¹³C NMR spectra for zinc(II) complex were obtained at room

temperature on a Varian 400 NMR spectrometer operating at 400 MHz (^1H) and 100 MHz (^{13}C). ^1H and ^{13}C NMR chemical shifts (δ) are reported in ppm and were referenced internally to residual solvent resonances (DMSO- d_6 : $\delta_{\text{H}} = 2.49$, $\delta_{\text{C}} = 39.4$ ppm). The conductivity measurements were performed using a Mettler Toledo Seven Easy conductivity meter, calibrated by the aid of a 1413 $\mu\text{S}/\text{cm}$ conductivity standard. Elemental analyses were carried out by the Atlantic Microlaboratory, Norcross, Georgia U.S.A.

Caution: Salts of perchlorate and their metal complexes are potentially explosive and should be handled with great care and in small quantities.

Syntheses of the complexes

$[\text{Ni}_2(\mu\text{-L}^{\text{Cl}}\text{O})(\mu_2\text{-OAc})_2](\text{PF}_6)\cdot 3\text{H}_2\text{O}$ (1). To a mixture of $\text{Ni}(\text{OAc})_2\cdot 4\text{H}_2\text{O}$ (0.100 g, 0.40 mmol) and 2,6-bis[bis(2-pyridylmethyl)amino]-4-chlorophenol (0.112 g, 0.20 mmol) dissolved in MeOH (25 mL), NH_4PF_6 (0.130 g, 0.80 mmol) was added. The resulting solution was heated on a steam-bath for 10 min, filtered while hot through celite and then allowed to stand at room temperature. After ca 3 h, the light blue single crystals which separated were collected by filtration, washed with propan-2-ol and Et_2O and then dried at room temperature (overall yield: 120 mg, 61%). Characterization for **1**: Calcd for $\text{C}_{36}\text{H}_{42}\text{ClF}_6\text{Ni}_2\text{N}_6\text{O}_8\text{P}$ (MM = 984.52 g/mol): C, 43.92; H, 4.30; N, 8.54%. Found: C, 44.23; H, 4.30; N, 8.57%. Selected FTIR bands (ν , cm^{-1}): 3432 (m,b) $\nu(\text{O-H})$, 1604 (vs) $\nu(\text{C=C})$; 1422 (m), $\nu(\text{C=N})$; 845 (vs) $\nu_{\text{as}}(\text{P-F})$. UV- VIS spectrum $\{\lambda_{\text{max}}$, nm (ϵ , $\text{M}^{-1}\text{cm}^{-1}$) $\}$ in CH_3CN : 490 (sh), 645 (11.5), ~ 960 (25.6, b). Molar conductivity in CH_3CN , $\Lambda_{\text{M}} = 131 \Omega^{-1} \text{cm}^2 \text{mol}^{-1}$.

$[\text{Ni}_2(\mu\text{-L}^{\text{Cl}}\text{O})(\mu_2\text{-OAc})_2](\text{ClO}_4)\cdot \text{CH}_3\text{COCH}_3$ (2). To a mixture of $\text{Ni}(\text{OAc})_2\cdot 4\text{H}_2\text{O}$ (0.100 g, 0.40 mmol) and 2,6-bis[bis(2-pyridylmethyl)amino]-4-chlorophenol (0.112 g, 0.20 mmol) dissolved in MeOH (25 mL), NaClO_4 (0.100 g, 0.80 mmol) was added. The resulting solution was heated on a steam-bath for 10 min, filtered while hot through celite and then allowed to stand at room temperature. The crude solid which separated was collected by filtration, washed with propan-2-ol and Et_2O and then dried at room temperature (overall yield: 105 mg, 56%). Recrystallization of the product from acetone afforded aqua-blue crystals suitable for X-ray structure determination. Characterization for **2**: Calcd for $\text{C}_{39}\text{H}_{42}\text{ClNi}_2\text{N}_6\text{O}_{10}$ (MM = 943.09 g/mol): C, 49.67; H, 4.49; N, 8.91%. Found: C, 48.28; H, 4.32; N, 9.15%. Selected FTIR bands (ν ,

cm^{-1}): 1604 (vs), 1593 (m) $\nu(\text{C}=\text{C})$; 1430 (s), 1415 (s), $\nu(\text{C}=\text{N})$; 1121 (s), 1095 (s) $\nu_{\text{as}}(\text{Cl}-\text{O})$. UV-VIS spectrum $\{\lambda_{\text{max}}, \text{nm} (\epsilon, \text{M}^{-1}\text{cm}^{-1})\}$ in CH_3CN : 490 (sh), 642 (7.2), ~955 (22,b). $\Lambda_{\text{M}}(\text{CH}_3\text{CN}) = 152 \Omega^{-1} \text{cm}^2 \text{mol}^{-1}$.

[Cu₂(μ -L^{Cl}O)(μ ₂-OAc)(ClO₄)](ClO₄) (3). A procedure similar to that described for **2** was used but Cu(OAc)₂·H₂O (0.100 g, 0.40 mmol) was used instead of Ni(OAc)₂·4H₂O. After one day, the green compound which separated was collected by filtration and was further recrystallized from MeOH. The green crystals which were collected by filtration, washed with propan-2-ol and Et₂O and then dried in air (overall yield: 120 mg, 61%). Characterization for **3**: Calcd for C₃₄H₃₃Cl₃Cu₂N₆O₁₁ (MM = 935.11 g/mol): C, 43.38; H, 3.56; N, 8.99%. Found: C, 43.52; H, 3.72; N, 8.56%. Selected FTIR bands (ν , cm^{-1}): 1637 (vs) $\nu(\text{C}=\text{C})$; 1439 (w), $\nu(\text{C}=\text{N})$; 1120 (m), 1108 (m), 1091 (m) $\nu_{\text{as}}(\text{Cl}-\text{O})$. UV-VIS spectrum $\{\lambda_{\text{max}}, \text{nm} (\epsilon, \text{M}^{-1}\text{cm}^{-1})\}$ in CH_3CN : 426 (465), ~800 (202,b). $\Lambda_{\text{M}}(\text{CH}_3\text{CN}) = 280 \Omega^{-1} \text{cm}^2 \text{mol}^{-1}$.

[Cu₂(μ -L^{Cl}O)(OAc)₂](PF₆)·H₂O (4). A procedure similar to that described for complex **3** but NH₄PF₆ (0.100g, 0.80 mmol) was used instead of NaClO₄. The crude solid which was separated in the following day was collected by filtration. Further recrystallized of the product from MeOH afforded blue crystals which were collected by filtration, washed with propan-2-ol and Et₂O and dried in air (overall yield: 120 mg, 63%). Characterization for **4**: Calcd for C₃₆H₃₈ClCu₂F₆N₆O₆P (MM = 958.25 g/mol): C, 45.12; H, 4.00; N, 8.77%. Found: C, 45.21; H, 4.01; N, 8.76%. Selected FTIR bands (ν , cm^{-1}): 3432 (s) $\nu(\text{O}-\text{H})$; 1612 (vs) $\nu(\text{C}=\text{C})$; 1587 (s), 1486 (w), 1459 (m), 1445 (s), 1398 (s) $\nu(\text{C}=\text{N})$; 842 (vs) $\nu_{\text{as}}(\text{P}-\text{F})$. UV-VIS spectrum $\{\lambda_{\text{max}}, \text{nm} (\epsilon, \text{M}^{-1}\text{cm}^{-1})\}$ in CH_3CN : 404 (713), ~670 (155,b). $\Lambda_{\text{M}}(\text{CH}_3\text{CN}) = 131 \Omega^{-1} \text{cm}^2 \text{mol}^{-1}$.

[Zn₂(μ -L^{Cl}O)(μ ₂-OAc)₂](PF₆) (5). A procedure similar to that described for complex **4** except Zn(OAc)₂·2H₂O (0.088 g, 0.40 mmol) was used instead of Cu(OAc)₂·H₂O. The crude solid which was separated in the following day was collected by filtration. Recrystallization of the product from MeOH afforded colorless long needles of X-ray quality. These were collected by filtration, washed with propan-2-ol and Et₂O and dried in air (overall yield: 170 mg, 90%). Characterization for **5**: Calcd for C₃₄H₃₇Cl₃Cu₂N₆O₁₃ (MM = 943.93 g/mol): C, 50.22; H, 4.46; N, 10.34%. Found: C, 49.93; H, 4.51; N, 10.28%. Selected FTIR bands (ν , cm^{-1}): 1604 (vs), 1574 (m), 1465 (m), 1429 (s), 843 (vs). UV-Vis spectrum $\{\lambda_{\text{max}}, \text{nm} (\epsilon, \text{M}^{-1}\text{cm}^{-1})\}$ in CH_3CN : 303 (2610). $\Lambda_{\text{M}}(\text{CH}_3\text{CN}) = 132 \Omega^{-1} \text{cm}^2 \text{mol}^{-1}$. ¹H NMR (DMSO-d₆, 400 MHz, δ in ppm): 2.00 (s, 3H, CH₃-acetate), 2.50 (s, 2H, H13), 3.34-3.38 (m, 6H, H13a, H13b, H22a, H22b, H11a, H11b), 3.69 (d,

1H, H12a), 3.75 (d, 1H, H12b), 4.07 (d, 1H, H20a), 4.41 (d, 1H, H20b), 6.63 (d, 1H, H7), 6.72 (s, 1H, H16), 7.17 (t, 1H, H4), 7.48 (t, 1H, H9), 7.54 (t, 1H, H8), 7.63 (d, 1H, H2), 8.03 (t, 1H, H3), 8.20 (d, 1H, H10), 8.69 (d, 1H, H5). ^{13}C NMR (DMSO- d_6 , 400 MHz): 24.84 (CH_3 -, acetate), 56.94 (C11), 58.31 (C12), 59.37 (C13), 117.59 (C5), 121.04 (C10), 122.99 (C9), 124.20 (C3), 124.41 (C8), 125.08 (C4), 129.57 (C9), 138.16 (C2), 139.56 (C7), 145.79 (C18), 147.29 (C16), 149.60 (C19), 154.44 (C15), 154.72 (C17), 160.55 (C14), 177.80 (-C=O, acetate). The atom numbering of the complex ion $[\text{Zn}_2(\mu\text{-L}^{\text{ClO}})(\mu_2\text{-OAc})_2]^+$ is shown in Chart 1.

$\text{Mn}_2(\text{L}^{\text{Cl}}\text{-O})(\mu_2\text{-OAc})_2(\text{ClO}_4)\cdot\text{H}_2\text{O}$ (6). A mixture containing $\text{Mn}(\text{ClO}_4)_2\cdot 6\text{H}_2\text{O}$ (0.150 g, 0.40 mmol) and 2,6-bis[bis(2-pyridylmethyl)amino]-4-chlorophenol (0.112 g, 0.20 mmol) dissolved in MeOH (25 mL) was heated on a steam bath for 10 min, then NaOAc (0.108 g, 0.80 mmol) was added followed by heating for another 10 min, filtered while hot through celite and then was allowed to stand at room temperature. In the following day, the off white long needles which separated were collected by filtration, washed with propan-2-ol and Et_2O and then dried at room temperature (overall yield: 72 mg, 40%). Anal. Calcd for **6**: $\text{C}_{36}\text{H}_{38}\text{Cl}_2\text{Mn}_2\text{N}_6\text{O}_{10}$ (MM = 895.53 g/mol): C, 48.28; H, 4.28; N, 9.38%. Found: C, 47.88; H, 4.16; N, 9.23%. Selected FTIR bands (ν , cm^{-1}): 3448 (w), 1589 (vs), 1427 (s), 1320 (w), 1093 (s). UV-VIS spectrum $\{\lambda_{\text{max}}$, nm (ϵ , $\text{M}^{-1}\text{cm}^{-1}$) in CH_3CN : 316 (3550), ~ 500 (sh). $\Lambda_{\text{M}}(\text{CH}_3\text{CN}) = 167 \Omega^{-1} \text{cm}^2 \text{mol}^{-1}$.

X-Ray crystal structure analysis

The X-ray single-crystal data of compounds **1-6** were collected on a Bruker-AXS APEX CCD diffractometer at 100(2) K. The crystallographic data, conditions retained for the intensity data collection and some features of the structure refinements are listed in Table S1 (see supplementary section). The intensities were collected with Mo- $\text{K}\alpha$ radiation ($\lambda = 0.71073 \text{ \AA}$). Data processing, Lorentz-polarization and absorption corrections were performed using APEX, and the SADABS computer programs.⁶⁸ The structures were solved by direct methods and refined by full-matrix least-squares methods on F^2 , using the SHELXTL⁶⁹ program package. All non-hydrogen atoms were refined anisotropically. The hydrogen atoms were located from difference Fourier maps, assigned with isotropic displacement factors and included in the final refinement cycles by use of HFIX (parent C atom) or DFIX (parent O atom) utility of the SHELXTL program. Molecular plots were performed with the Mercury program.⁷⁰

Magnetic Measurements

Magnetic data of nickel (**1** and **2**) and manganese (**6**) complexes were measured with a PPMS Dynacool VSM magnetometer ($T = 1.9\text{--}300\text{ K}$ at $B = 0.1/1\text{ T}$; $B = 0\text{--}9\text{ T}$ at $T = 2, 5$ and 10 K). The copper complexes (**3** and **4**) were measured with a MPMS XL7 SQUID magnetometer ($T = 1.9\text{--}300\text{ K}$ at $B = 1\text{ T}$; $B = 0\text{--}5\text{ T}$ at $T = 2$ and 5 K). The magnetic data were corrected for diamagnetic susceptibilities and the signal of the sample holder.

DFT Calculations

The DFT calculations were performed with the ORCA 3.0.3 computational package.⁷¹ The hybrid B3LYP functional⁷² and the polarized triple- ζ quality basis set def2-TZVP(-f) proposed by Ahlrichs and co-workers was used for all atoms.⁷³ The calculations utilized the RI approximation with the decontracted auxiliary def2-TZV/J Coulomb fitting basis sets and the chain-of-spheres (RIJCOSX) approximation to exact exchange as implemented in ORCA.⁷⁴ Increased integration grids (Grid5 in ORCA convention) and tight SCF convergence criteria were used in all calculations. The spin densities were visualized with the program VESTA 3.⁷⁵

DNA study

Interactions of the complexes with plasmid DNA

To determine the nuclease activity of the complexes **1-5**, 300 ng (i.e. $23.1\text{ }\mu\text{M}$ of base pairs) in the $20\text{ }\mu\text{L}$ of reaction mixture of the native supercoiled pUC19 plasmid DNA was incubated with different concentrations of the tested complexes which were dissolved in 25% (v/v) acetonitrile at $37\text{ }^\circ\text{C}$ and allowed to interact for 2 h. Immediately after that, the samples were then quickly cooled to $4\text{ }^\circ\text{C}$ and mixed with gel loading buffer [containing 30% (v/v) glycerol, 0.25% (w/v) bromophenol blue] and subsequently loaded on 0.8% (w/v) agarose gel in TBE buffer (containing 45 mM Tris-borate buffer and 1 mM EDTA) impregnated with $0.15\text{ }\mu\text{g/mL}$ of ethidium bromide (EtBr). The electrophoreogram was analyzed by the AlphaEaseFC version 4.0.0.34 software (Alpha Innotech, USA) and the relative amounts of the supercoiled circular (SC-form), single-strand nicked (OC-form) and linear (L-form) forms were evaluated. The quantification of SC-form of plasmid DNA was corrected by a factor of 1.47.³⁹

Effect of incubation time on the interaction of complex **3** with plasmid DNA

To evaluate the effect of incubation time on the cleaving activity of the compounds, Cu(II) complex **3** was selected as a model compound. The compound was incubated in the concentrations

of 300 and 30 μM with 300 ng of supercoiled plasmid DNA for 2, 4, 6, and 22 h. After the incubation, the samples were analyzed by gel electrophoresis as described above.

Effect of oxidative scavengers and inhibitors on the interactions of Ni(II) complexes with plasmid DNA

The Ni(II) complexes **1** and **2** were selected for the determination whether their interactions with supercoiled plasmid DNA could be modulated in the presence of different inhibitors. Therefore, the ROS scavengers DMSO, and KI,^{39,46(a)} the metal competitor MgSO_4 and highly efficient metal chelator EDTA were added in the molar ratio of 1:1 with 300 and 33 μM of the complexes and these were incubated with 300 ng of plasmid DNA at 37 °C for 2 h in a similar manner as described above.

Kinetics of the phosphodiester hydrolysis

Phosphodiester hydrolysis activity was probed for complexes **1**, **3** and **5**. BDNPP was used as a phosphodiester model substrate in the assay. It was synthesized following a published procedure with minor modifications.⁷⁶ Cleavage of BDNPP was followed spectrophotometrically by monitoring the generated product, 2,4-dinitrophenolate, by its strong absorption at 400 nm ($\epsilon = 12,100 \text{ M}^{-1}\text{cm}^{-1}$). The spectra were recorded at 25 °C with a JASCO V-570 spectrophotometer in a 10 mm or a 2 mm quartz cuvettes. All measurements were carried out in 1:1 acetonitrile-buffer mixtures and performed in triplicates. The aqueous buffer consisted of 2-(N-morpholino)-ethanesulfonic acid (MES) (50 mM; pH range: 5.5–6.7), 4-(2-hydroxyethyl)piperazine-1-ethanesulfonic acid (50 mM; pH range: 6.8 - 8.2), 2-(cyclohexylamino)ethanesulfonic acid (CHES) (50 mM; pH range: 8.6 - 10.0), 3-(cyclohexylamino)-1-propanesulfonic acid (CAPS) (50 mM; pH range: 9.7 – 11.1) and lithium perchlorate (250 mM) for ionic strength control. The desired pH of the buffers was adjusted by addition of aqueous sodium hydroxide solution. Subsequent treatment with Chelex® (Chelex 100 sodium form) overnight and filtration with 45 μm syringe filters ensured the absence of metal ions in the buffer solutions. BDNPP was initially prepared as a 15 mM stock solution in acetonitrile and the complex stock solutions were 1 mM in acetonitrile. The complex was allowed to equilibrate in the acetonitrile-buffer mixture for one minute prior to addition of the substrate. When the substrate was added to the reaction mixture the starting hydrolysis activity was monitored in the time between 15 and 195 seconds and analyzed by linear regression. For each experiment autohydrolysis assays were conducted by measuring the hydrolysis rate under the same conditions, but without complex, and were subtracted from the

derived data. The pH dependence assays contained the complex at 0.02 mM and BDNPP at 2.5 mM in the cuvette. The substrate concentration dependence assays were 0.04 mM in complex. The experimental data obtained were fitted by the Origin (OriginLab) program. Studies of the TON were conducted at 10 μ M in complex and 3 mM in BDNPP. Samples were taken at various intervals during the experiment, diluted with solvent (final concentration: 0.5 nM in complex and 0.15 mM in BDNPP), and their UV-vis spectra were recorded. The increase in the absorbance at 400 nm, assigned to 2,4-dinitrophenolate, was monitored over time and TON values calculated using the Beer-Lambert Law.

Conclusions

Six dinuclear metal(II)-acetato complexes $[\text{Ni}_2(\mu\text{-L}^{\text{Cl}}\text{O})(\mu_2\text{-OAc})_2](\text{PF}_6)\cdot 3\text{H}_2\text{O}$ (**1**), $[\text{Ni}_2(\mu\text{-L}^{\text{Cl}}\text{O})(\mu_2\text{-OAc})_2](\text{ClO}_4)\cdot \text{CH}_3\text{COCH}_3$ (**2**), $[\text{Cu}_2(\mu\text{-L}^{\text{Cl}}\text{O})(\mu_2\text{-OAc})(\text{ClO}_4)](\text{ClO}_4)$ (**3**), $[\text{Cu}_2(\mu\text{-L}^{\text{Cl}}\text{O})(\text{OAc})_2](\text{PF}_6)\cdot \text{H}_2\text{O}$ (**4**), $[\text{Zn}_2(\mu\text{-L}^{\text{Cl}}\text{O})(\mu_2\text{-OAc})_2](\text{PF}_6)$ (**5**) and $[\text{Mn}_2(\text{L}^{\text{Cl}}\text{-O})(\mu_2\text{-OAc})_2](\text{ClO}_4)\cdot \text{H}_2\text{O}$ (**6**) have been synthesized in order to test their efficiencies in catalyzing the P-O bonds in DNA and in promoting the hydrolysis of BDNPP. These complexes were structurally and magnetically characterized. The backbone of all complexes consists of 2,6-bis[bis(2-pyridylmethyl)aminomethyl]-4-chlorophenolate ($\text{L}^{\text{Cl}}\text{-O}^-$) linking the two metal ions through the deprotonated phenolate group, the acetate ligands are further bridging the metal ions in complexes **1**, **2**, **3**, **5** and **6** but are simple monodentate donors in **4**. The magnetic measurements revealed antiferromagnetic coupling for complexes **1**, **2**, **4** and **6**, and ferromagnetic coupling in **3**, and these results were supported by the DFT calculations.

The hydrolysis of the phosphodiester bis(2,4-dinitrophenol)phosphate (BDNPP), used as a model substrate for the P-O bond cleavage in DNA, was examined with complexes **1**, **3** and **5** over the pH range 5.5-10.5 at 25 $^\circ\text{C}$. Michaelis-Menten kinetics (pH = 7 and 10.5) showed that catalytic efficiencies $k_{\text{cat}}/K_{\text{M}}$ decrease in the order Ni(II), **1** > Zn(II), **5** > Cu(II), **3**. Parallel to the phosphatase reactivity study, the nuclease activity of complexes **1-5** were employed for studying the supercoiled plasmid ds-DNA cleavage under the physiological conditions. Surprisingly, none of the complexes showed any sign of cleavage activity but instead only the two nickel complexes **1** and **2** revealed a strong ability to unwound the supercoiled plasmid ds-DNA. These results raise a question about the validity of a direct comparison model metal complexes used for the hydrolysis

of phosphodiester with DNA cleavage, where two mechanistic pathways (hydrolysis and oxidative cleavage) exist. In addition to the present results, $[\text{Zn}(\text{TPA})(\text{H}_2\text{O})]^{2+}$ (TPA = tris(2-pyridylmethyl)amine) was shown to exhibit enhanced phosphodiester hydrolysis rate⁷⁷ but the corresponding catalytic cleavage reaction for DNA was insignificant.^{46(b)}

Comparative studies for supercoiled ds-DNA cleavage efficiency by a number of metal complexes, when different metals exist in the same coordination environment and are bound to the same ligand, have been performed.^{42(a),46(b)} For example in the cleavage of DNA by the structurally characterized hexa-coordinate complexes $[\text{M}(\text{bpa})(\text{NO}_3)]^+$, where bpa = N-(2-ethoxyetanol)-bis(2-picolyl)amine, the efficiency decreased in the order: $\text{Cu}(\text{II}) > \text{Co}(\text{II}) > \text{Zn}(\text{II}) \approx \text{Ni}(\text{II})$ ^{42(a)} and in a comparable study using the five-coordinate $[\text{M}(\text{TPA})(\text{H}_2\text{O})]^{2+}$, the reactivity order was $\text{Co}(\text{II}) > \text{Cu}(\text{II}) \gg \text{Zn}(\text{II})$.^{46(b)} These two sets of data demonstrate that the observed reactivity is not attributed to a specific metal ion nor to the lability of metal ions.⁷⁸ In addition, our recent work on the DNA cleavage by a series of sterically hindered TBP Co(II) complexes derived from the substituted N4-tripod TPA³⁹ and on the dinuclear Cu(II)-bdpaT^{Cl} complexes, where bdpaT^{Cl} = 2-chloro-4,6-bis(di-2-picolylamino)-1,3,5-triazine,³⁶ showed that the steric environment imposed by the ligands around the central metal ions has a strong influence on suppressing the approach of DNA to the metal center and this may lower or even inhibit the reactivity of DNA cleavage.^{36,39} However, it is important to mention that this may not be the case in the hydrolysis of simple phosphodiester as these molecules have a very small size compared to DNA. Therefore, aside from the mechanistic complications in the DNA cleavage reactions, the observed lack of reactivity of complexes **1-5** in the DNA cleavage reactions and the observed efficiency by complexes **1** and **5** in promoting the hydrolysis of BDNPP may be due to the large steric effect imposed by the coordinated organic ligands which prohibit the ds-DNA from closely approaching the metal centers while this presents no problem for BDNPP. In conclusion, careful attention must be paid for the results in which metal complexes are used to mimic the hydrolysis of simple phosphodiester compounds as “*model systems*” for the natural biological phosphoesters, DNA or RNA.

Acknowledgements

S. S. M. acknowledges the financial support of this research by the Department of Chemistry-University of Louisiana at Lafayette. R. H., J. H. and Z. T. gratefully thank the National Program

of Sustainability I (LO1305) of the Ministry of Education, Youth and Sports of the Czech Republic for financial support. F. A. M. acknowledges the support by NAWI Graz. S. B. and P. C. gratefully acknowledge support by the German Science Foundation (DFG), the Deutscher Akademischer Austauschdienst (DAAD) and the University of Heidelberg.

References

- (a) S. S. Massoud, M. Spell, C. Ledet, T. Junk, R. Herchel, R. C. Fischer, Z. Travnicek, F. A. Mautner, *Dalton Trans.*, 2015, 44, 2110-2121; (b) S. S. Massoud, T. Junk, F. R. Louka, R. Herchel, Z. Travnicek, R. C. Fischer, F. A. Mautner, *RSC Advances*, 2015, 5, 87139-87150.
- G. Ambrosi, M. Formica, V. Fusi, L. Giorgi, M. Micheloni, *Coord. Chem. Rev.*, 2008, 252, 1121-1152.
- (a) S. Svane, F. Kryuchkov, C. J. Lennarston, C. K. McKenzie, F. Kjeldsen, *Angew. Chem., Int. Ed.*, **2012**, 51, 3216-3219; (b) R. K. Edgal, A. D. Bond, C. J. Mckenzie, *Dalton Trans.*, 2009, 3833-3839; (c) R. K. Edgal, F. B. Larsen, A. D. Bond, C. J. Mckenzie, *Inorg. Chim. Acta*, 2005, 358, 376-382.
- (a) A. Boisen, A. Hazell, C. J. Mckenzie, *Chem. Commun.*, 2001, 2136-2137; (b) P. Dalgaard, A. Hazell, C. J. McKenzie, B. Moubaraki, K. S. Murray, *Polyhedron*, 2000, 19, 1909-1015; (c) H. Adams, D. Bradshaw, D. E. Fenton, *Inorg. Chim. Acta*, 2002, 332, 195-200.
- (a) A. S. Borovik, M. P. Hendrich, T. R. Holman, E. Munck, V. Papaefthymiou, L. Que Junior, *J. Am. Chem. Soc.*, 1990, 112, 6031-6038; (b) A. S. Borovik A. S.; L. Que Junior *J. Am. Chem. Soc.*, 1988, 110, 2345-2347.
- F. R. Xavier, A. Neves, A. Casellato, R. A. Peralta, A. J. Bortoluzzi, B. Szpoganicz, P. C. Severino, H. Terenzi, Z. Tomkowicz, S. Ostrovsky, W. Haase, A. Ozarowski, J. Krzystek, J. Telser, G. Schenk, L. R. Gahan, *Inorg. Chem.*, 2009, 48, 7905-7921.
- (a) F. Michel, P. Torelli, St., F. Thomas, C. Duboc, C. Philouze, S. Belle, E. Hamman, S. Saint-Aman, J. L. Pierre, *Angew. Chem. Int. Ed.*, 2005, 44, 438-441; (b) R. C. Holz, M. J. Brink, *Inorg. Chem.*, 1994, 33, 4609-4610.
- S. Torelli, C. Belle, I. Gautier-Luneau, J. L. Pierre, E. Saint-Aman, J. M. Latour, L.-L. Pape, D. Luneau, *Inorg. Chem.*, 2000, 39, 3526-3536.
- M. Jarenmark, M. Haukka, S. Demeshko, F. Tuzek, L. Zuppiroli, F. Meyer, E. Nordlander, *Inorg. Chem.*, 2011, 50, 3866-3887.
- A. Neves, M. Lanznaster, A. J. Bortoluzzi, R. A. Peralta, A. Casellato, E. E. Castellano, P. Herrald, M. J. Riley, G. Schenk, *J. Am. Chem. Soc.*, 2007, 129, 7486-7487.
- S. S. Massoud, T. Junk, R. Herchel, Z. Travnicek, M. Mikuriya, R. C. Fischer, F. A. Mautner, *Inorg. Chem. Commun.*, 2015, 60, 1-3; (b) S. S. Massoud, T. Junk, M. Mikuriya, N. Naka, F. A. Mautner, *Inorg. Chem. Commun.*, 2014, 50, 48-50.
- K. D. Karlin, Z. Tyeklár, A. Farooq, M. S. Haka, P. Ghosh, R. W. Cruse, Y. Gultneth, J. C. Hayes, P. J. Toscano, J. Zubieta, *Inorg. Chem.*, 1992, 31, 1436-1451.
- L. J. Daumann, J. A. Larrabee, P. Comba, G. Schenk, L. R. Gahan, *Eur. J. Inorg. Chem.*, 2013, 3082-3089.

- 14 S. J. Smith, C. J. Noble, R. C. Palmer, G. R. Hanson, G. Schenk, L. R. Gahan, M. J. Riley, *J. Biol. Inorg. Chem.*, 2008, 13, 499-510.
- 15 T. P. Camargo, F. F. Maia, C. Chaves, B. de Souza, A. J. Bortoluzzi, N. Castilho, N.; T. Bortolotto, H. Terenzi, E. E. Castellano, W Haase, Z. Tomkowicz, R. A. Peralta, A. Neves, *J. Inorg. Biochem.*, 2015, 146, 77-88.
- 16 R. L. Lomoth, P. Huang J. Zheng, L. Sun, L. Hammarström, B. Akermark, S. Styring, *Eur. J. Inorg. Chem.*, 2002, 5965-2974.
- 17 Y. Gultneh, Y. T. Tesema, T. B. Yisgedu, R. J. Butcher, G. Wang, G. T. Yee, *Inorg. Chem.*, 2006, 45, 3023-3033.
- 18 M. Ghiladi, C. K. Mckenzie, A. Meler, A. K. Powell, J. Ulstrup, S. Wocadlo, *J. Chem. Soc., Dalton Trans.*, 1997, 4011-4018.
- 19 P. V. Bernhardt, S. Bosch, P. Comba, L. R. Gahan, G. R. Hanson, V. Mereacre, C. J. Noble, A. K. Powell, G. Schenk, H Wadepohl, *Inorg. Chem.*, 2015, 54, 7249-7263.
- 20 P. Comba, L. R. Gahan, V. Mereacre, G. R. Hanson, A. K. Powell, G. Schenk, M. Zajaczkowski-Fischer, *Inorg. Chem.*, 2012, 51, 12195-12209.
- 21 S. Bosch, P. Comba, L. R. Gahan, G. Schenk, *Inorg. Chem.*, 2014, 53, 9036-9051.
- 22 B. Das, H. Daver, M. Pyrkosz-Bulska, E. Perscha, S. K. Barman, R. Mukherjee, E Gumienka-Kontecka, M. Jarenmark, F. Himo, E. Nordlander, *J. Inorg. Biochem.*, 2014, 132, 6-17.
- 23 L. J. Daumann, P. Comba, J. A. Larrabee, G. Schenk, R. Stranger, G. Cavigliasso, L. R. Gahan, *Inorg. Chem.*, 2013, 52, 2029-2043.
- 24 D. Montagner, V. Gandin, C. Marzano, A. Erxleben, *Eur. J. Inorg. Chem.*, 2014, 4084-4092.
- 25 N. A. Rey, A. Neves, A. J. Bortoluzzi, C. T. Pich, P. H. Terenzi, *Inorg. Chem.*, 2007, 46, 348-350.
- 26 (a) G. K. Schroeder, C. Lad, P. Wyman, N. H. Williams, R. Wolfenden, *Proc. Natl. Acad. Sci. U.S.A.*, 2006, 103, 4052-4255; (b) J. A. Cowan, *Chem. Rev.*, 1998, 98, 1067-1088.
- 27 P. Hendry, A. M. Sargeson, *Progress Inorg. Chem.: Bioinorganic Chemistry* (Ed. S. Lippard) 1990, 38, 201-258.
- 28 J. A. Cowan, *Nucleic Acids and Molecular Biology*, 2004, 14, 339-360.
- 29 C. Liu, M. Wang, T. Zhang, H. Sun, *Coord. Chem. Rev.*, 2004, 248, 147-168.
- 30 P. Molenveld, J. F. J. Engbersen, D. N. Reinhoudt, *Chem. Soc. Rev.*, 2000, 29, 75-86.
- 31 (a) M. Pitie, C. Boldron, G. Pratviel, (Eds: R. van Eldick, J. Reedijk) *Advances in Inorganic Chemistry*, 2006, 58, 77-130; (b) G. Pratviel, A. Bernadou, B. Meunier, (Ed. G. A. Sykes) *Advances in Inorganic Chemistry*, 1997, 45, 251-312, Academic Press, London.
- 32 (a) Y. Jin, M. A. Lewis, N. H. Gokhale, E. C. Long, J. A. Cowan, *J. Am. Chem. Soc.*, 2007, 129, 8353-8361; (b) Y. Jin, J. A. Cowan, *J. Am. Chem. Soc.*, 2005, 127, 8408-8415.
- 33 (a) L. Qian, W. R. Browne, G. Roelfes, *Inorg. Chem.*, 2011, 50, 8318-8325; (b) Q. Li, W. R. Browne, G. Roelfes, *Inorg. Chem.*, 2010, 49, 11009-11017.
- 34 (a) D.-D. Li, J.-L. Tian, W. Gu, X. Liu, H.-H. Zeng, S.-P. Yan, *J. Inorg. Biochem.*, 2011, 105, 894-901; (b) D.-D. Li, F.-P. Huang, G.-J. Chen, Y.-C. Gao, J.-L. Tian, W. Gu, X. Liu, S.-P. Yan, *J. Inorg. Biochem.*, 2010, 104, 431-441.
- 35 (a) H. Prakash, A. Shodal, H. Yasui, H. Sakurai, H.; S. Hirota, *Inorg. Chem.*, 2008, 47, 5045-5047; (b) H. Li, X.-Y. Le, D. W. Pang, H. Deng, Z.-H. Xu, Z.-H. Lin, *J. Inorg. Biochem.*, 2005, 99, 2240-2247.
- 36 S. S. Massoud, F. R. Louka, W. Xu, R. Perkins, R. Vicente, J. H. Albering, F. A. Mautner, *Eur. J. Inorg. Chem.* 2011, 3469-3479.

- 37 O. I. Aruoma, B. Halliwell, M. Dizdaroglu, *J. Biol. Chem.*, 1989, 264, 13024-13028.
- 38 Q. Jiang, N. Xiao, P. Shi, Y. Zhu, Z. Guo, *Coord. Chem. Rev.*, 2007, 251, 1951-1972.
- 39 S. S. Massoud, R. S. Perkins, F. R. Louka, W. Xu, A. Le Roux, Q. Dutercq, R. C. Fischer, F. A. Mautner, M. Handa, Y. Hiraoka, G. L. Kreft, T. Bortolotto, H. Terenzi, *Dalton Trans.*, 2014, 43, 10086-10103.
- 40 K. E. Erkkila, D. T. Odom, J. K. Barton, *Chem. Rev.*, 1999, 99, 2777-2796.
- 41 M. S. Deshpande, A. A. Kumbhar, A. S. Kumbhar, *Inorg. Chem.*, 2007, 46, 5450-5452.
- 42 (a) S. I. Kirilin, C. M. Happel, S. Hrubanova, T. Weyhermüller, C. Klein, N. M. Nottle, *Dalton Trans.*, 2004, 1201-1207; (b) T. Itoh, H. Hisada, T. Sumiya, T. Hosono, Y. Usui, Y. Fujii, *Y. Chem. Commun.*, 1997, 677-678.
- 43 J. T. Wang, Q. Xia, X.-H. Zheng, H.-Y. Chen, H. Chao, Z.-W. Mao, L.-N. Ji, *Dalton Trans.*, 2010, 39, 2128-2136.
- 44 S. Dhar, P. A. N. Reddy, A. R. Chakravarty, *Dalton Trans.*, 2004, 697-698.
- 45 J. He, J. Sun, Z. W. Mao, L. N. Ji, H. Z. Sun, *J. Inorg. Biochem.*, 2009, 103, 851-856.
- 46 (a) S. S. Massoud, R. S.; Perkins, K. D. Knierim, S. P. Comiskey, K. H. Otero, C. L. Michel, W. M. Juneau, J. H. Albering, F. A. Mautner, W. Xu, *Inorg. Chim. Acta*, 2013, 399, 177-184; (b) W. Xu, F. A. Craft, P. R. Fontenot, B. Marion, K. D. Knierim, J. H. Albering, F. A. Mautner, S. S. Massoud, *Inorg. Chim. Acta*, 2011, 373, 159-166.
- 47 G. Barone, A. Terenzi, A. Lauria, A. M. Almerico, J. M.; Leal, N. Busto, B. García, *Coord. Chem. Rev.*, 2013, 257, 2848-2862.
- 48 A. Terenzi, C. Ducani, L. Male, G. Baroneb, M. Hannon, *J. Dalton Trans.*, 2013, 42, 11220-11226.
- 49 (a) A. J. Clarke, N. Yamamoto, P. Jensen, T. W. Hambley, *Dalton Trans.*, 2009, 10787-10798; (b) A. Hille, I. Ott, A. Kitanovic, I. Kitanovic, H. Alborzinia, E. Lederer, S. Wolf, N. Metzler-Nolte, S. Schafer, W. S. Sheldrick, C. Bischof, U. Schatzschneider, R. Gust, *R. J. Biol. Inorg. Chem.*, 2009, 14, 711-725.
- 50 A. Arola-Arnal, J. Benet-Buchholz, S. Neidle, R. Vilar, *Inorg. Chem.*, 2008, 47, 11910-11919.
- 51 M. J. Hannon, *Chem. Soc. Rev.*, 2007, 36, 280-295.
- 52 R. Martinez, L. Chacon-Garcia, *Curr. Med. Chem.*, 2005, 12, 127-151.
- 53 B. M. Zeglis, V. C. Pierre, J. K. Barton, *Chem. Commun.*, 2007, 4565-4579.
- 54 (a) G. L. Miessler, P. J. Fischer, D. A. Tarr, *Inorg. Chem.*, 5th, Pearson, Boston, USA, 2014, p. 412-431; (b) C. E. Housecroft A. G. Sharpe, *Inorg. Chem.*, 4th edn, Pearson, Harlow, England, 2012, p. 687-697.
- 55 B. J. Hathaway, in *Comprehensive Coordination Chemistry*, ed. G. Wilkinson, R. D. Gillard, J. A. McCleverty, Pergamon Press, Oxford, England, 1987, vol. 5, p. 533.
- 56 (a) S. S. Massoud, F. R. Louka, R. N. David, M. J. Dartez, Q. L. Nguyn, N. J. Labry, R. C. Fischer, F. A. Mautner, *Polyhedron*, 2015, 90, 258-265; (b) S. S. Massoud, F. R. Louka, Y. K. Obaid, R. Vicente, J. Ribas, R. C. Fischer, F. A. Mautner, *Dalton Trans.*, 2013, 42, 3968-3978; (c) S. S. Massoud, L. Le Quan, K. Gatterer, J. H. Albering, R. C. Fischer, F. A. Mautner, *Polyhedron*, 2012, 31, 601-606; (d) F. A. Mautner, R. Vicente, S. S. Massoud, *Polyhedron*, 2006, 25, 1673-1680; (e) U. Mukhopadhyay, I. Bernal, S. S. Massoud, F. A. Mautner, *Inorg. Chim. Acta*, 2004, 357, 3673-3682.
- 57 A. W. Addison, T. N. Rao, J. Reedijk, J. V. Rijn, G. C. Verschoor, *J. Chem. Soc., Dalton Trans.*, 1984, 1349-1356.
- 58 R. Boča, *Theoretical Foundations of Molecular Magnetism*, Elsevier: Amsterdam, 1999.

- 59 (a) E. Ruiz, J. Cano, S. Alvarez, P. Alemany, *J. Comput. Chem.* 1999, 20, 1391-1400; (b) E. Ruiz, A. Rodríguez-Forteza, J. Cano, S. Alvarez, P. Alemany, *J. Comput. Chem.* 2003, 24, 982-989.
- 60 (a) K. Yamaguchi, Y. Takahara, T. Fueno, in *Applied Quantum Chemistry*, ed. V. H. Smith, Dordrecht, Reidel, Dordrecht 1986, p. 155-184; (b) T. Soda, Y. Kitagawa, T. Onishi, Y. Takano, Y. Shigeta, H. Nagao, Y. Yoshioka, K. Yamaguchi, *Chem. Phys. Lett.*, 2000, 319, 223-230.
- 61 L. R. Gahan, S. J. Smith, A. Neves, G. Schenk, *Eur. J. Inorg. Chem.*, 2009, 2745-2758.
- 62 D. Desbouis, I. P. Troitsky, M. J. Belousoff, L. Spiccia, B. Graham, *Coord. Chem. Rev.*, 2012, 256, 897-937.
- 63 R. Peralta, A. J. Bortoluzzi, B. de Souza, R. Jovito, F. R. Xavier, R. A. A. Couto, A. Casellato, F. Nome, A. Dick, L. R. Gahan, G. Schenk, G. R. Hanson, F. C. S. de Paula, E. C. Pereira-Maia, S. Machado, P. C. Severino, C. Pich, F. L. Fischer, H. Terenzi, E. E. Castellano, A. Neves, M. J. Riley, *Inorg. Chem.*, 2010, 49, 11421-11438.
- 64 I. H. Segel, *Enzyme Kinetics - Behavior and Analysis of Rapid Equilibrium and Steady-State Enzyme Systems*. Wiley-VCH, New York, 1975.
- 65 A. Kantacha, R. Buchholz, S. Smith, G. Schenk, L. R. Gahan, *J. Biol. Inorg. Chem.*, 2011, 16, 2011, 25-32.
- 66 (a) L. J. Daumann, L. Marty, G. Schenk, L. R. Gahan, *Dalton Trans.*, 2013, 42, 9574-9584; (b) L. J. Daumann, L. R. Gahan, P. Comba, G. Schenk, *Inorg. Chem.*, 2012, 51, 7669-7681.
- 67 S. Anbu, M. Kandaswamy, *Inorg. Chim. Acta*, 2012, 385, 45-52.
- 68 (a) Bruker (2005) SAINT v. 7.23; Bruker AXS Inc., Madison, Wisconsin, USA; (b) Sheldrick, G. M. (2001), SADABS v. 2. University of Goettingen, Germany.
- 69 G. M. Sheldrick, *Acta Crystallogr.*, 2008, A64, 112-122.
- 70 C. F. Macrae, P. R. Edington, P. McCabe, E. Pidcock, G. P. Shields, R. Taylor, T. Towler, J. van de Streek, *J. Appl. Cryst.*, 2006, 39, 453-457.
- 71 F. Neese, *WIREs Comput. Mol. Sci.* 2012, 2, 73-78.
- 72 (a) C. Lee, W. Yang, R. G. Parr, *Phys. Rev. B* 1988, 37, 785-789; (b) A. D. Becke, *J. Chem. Phys.*, 1993, 98, 1372-1377; (c) A. D. Becke, *J. Chem. Phys.*, 1993, 98, 5648-5652; (d) P. J. Stephens, F. J.; Devlin, C. F. Chabalowski, M. J. Frisch, *J. Phys. Chem.*, **1994**, 98, 11623-11627.
- 73 (a) A. Schafer, H. Horn, R. Ahlrichs, *J. Chem. Phys.*, 1992, 97, 2571-2577; (b) A. Schafer, C. Huber, R. Ahlrichs, *J. Chem. Phys.*, **1994**, 100, 5829-5835; (c) F. Weigend, R. Ahlrichs, *Phys. Chem. Chem. Phys.*, 2005, 7, 3297-3305.
- 74 (a) F. Neese, F. Wennmohs, A. Hansen, U. Becker, *Chem. Phys.*, 2009, 356, 98-109; (b) R. Izsak, F. Neese, *J. Chem. Phys.*, 2011, 135, 144-150.
- 75 K. Momma, F. Izumi, *J. Appl. Cryst.*, 2011, 44, 1272-1276.
- 76 C. A. Bunton, S. J. Farber, *J. Org. Chem.*, 1969, 34, 767-772.
- 77 G. Feng, J. C. Mareque-Rivas, R. T. M. de Rosales, N. H. Williams, *J. Am. Chem. Soc.*, 2005, 127, 13470-13471.
- 78 H. Krüger, *Chem. Soc. Rev.* 1982, 11, 227-255.

Fig. 1

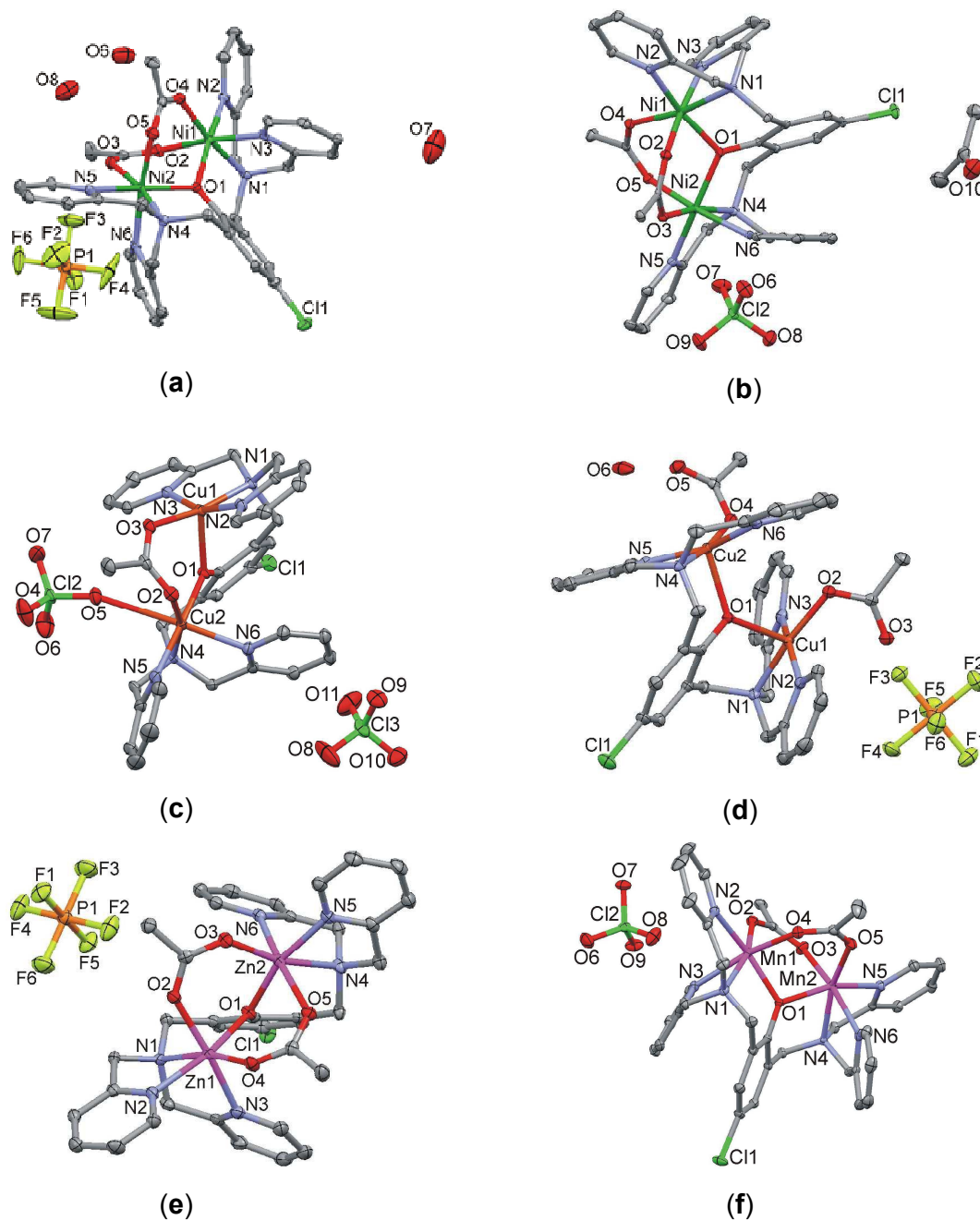


Fig. 1. Perspective views of complexes **1** - **6** with partial atom numbering schemes: (a) $[\text{Ni}_2(\mu\text{-L}^{\text{ClO}})(\mu_2\text{-OAc})_2](\text{PF}_6) \cdot 3\text{H}_2\text{O}$ (**1**), (b) $[\text{Ni}_2(\mu\text{-L}^{\text{ClO}})(\mu_2\text{-OAc})_2](\text{ClO}_4) \cdot \text{CH}_3\text{COCH}_3$ (**2**), (c) $[\text{Cu}_2(\mu\text{-L}^{\text{ClO}})(\mu_2\text{-OAc})(\text{ClO}_4)](\text{ClO}_4)$ (**3**), (d) $[\text{Cu}_2(\mu\text{-L}^{\text{ClO}})(\text{OAc})_2](\text{PF}_6) \cdot \text{H}_2\text{O}$ (**4**), (e) $[\text{Zn}_2(\mu\text{-L}^{\text{ClO}})(\mu_2\text{-OAc})_2](\text{PF}_6)$ (**5**) and (f) $[\text{Mn}_2(\text{L}^{\text{Cl-O}})(\mu_2\text{-OAc})_2](\text{ClO}_4) \cdot \text{H}_2\text{O}$ (**6**).